# L-DOPA dioxygenase activity on 6-substituted dopamine analogs

Alexander M. Goldberg<sup>†2</sup>, Miranda K. Robinson<sup>†2</sup>, Erykah S. Starr<sup>†</sup>, Ryan N. Marasco<sup>†</sup>, Alexa C. Alana<sup>†</sup>, C. Skyler Cochrane<sup>†</sup>, Kameron L. Klugh<sup>†</sup>, David Strzeminski<sup>2</sup>, Muxue Du<sup>2</sup>, Keri L. Colabroy<sup>2</sup>\*, Larryn W. Peterson<sup>†</sup>\*

<sup>1</sup>Department of Chemistry, Rhodes College, 2000 North Parkway, Memphis, TN 38112

<sup>2</sup>Department of Chemistry, Muhlenberg College, 2400 Chew St, Allentown, PA, 18104

#### **Author information**

#### Corresponding authors

\*Rhodes College, 2000 North Parkway, Memphis, TN, 38112. Email: <a href="mailto:petersonl@rhodes.edu">petersonl@rhodes.edu</a>

\*Muhlenberg College, 2400 Chew St, Allentown, PA 18104. Email: kericolabroy@muhlenberg.edu

#### Orcid

Keri L. Colabroy 0000-0002-8045-8403 Larryn W. Peterson 0000-0003-4448-9154

#### **Funding**

This work was funded by National Science Foundation Grant CHE 1708237 (K.L.C.) and 1708234 (L.W.P.)

<sup>&</sup>lt;sup>†</sup>These individuals contributed equally to this work.

## **Abstract**

Dioxygenase enzymes are essential protein catalysts for the breakdown of catecholic rings, structural components of plant woody tissue. This powerful chemistry is used in nature to make antibiotics, other bioactive materials or degrade plant material, but we have a limited understanding of the breadth and depth of substrate space for these potent catalysts. Here we report steady-state and pre-steady state kinetic analysis of dopamine derivatives substituted at the 6-position as substrates of L-DOPA dioxygenase, and an analysis of that activity as a function of the electron withdrawing nature of the substituent. Steady-state and pre-steady state kinetic data demonstrate the dopamines are impaired in binding and catalysis with respect to the co-substrate molecular oxygen, which likely afforded spectroscopic observation of an early reaction intermediate, the semiguinone of dopamine. The reaction pathway of dopamine in the pre-steady state is consistent with a non-productive binding mode of oxygen at the active site. Despite these limitations, L-DOPA dioxygenase is capable of binding all the dopamine derivatives and catalyzing multiple turnovers of ring cleavage for dopamine, 6-bromodopamine, 6-carboxydopamine, and 6-cyanodopamine. 6-Nitrodopamine was a single turnover substrate. The variety of substrates accepted by the enzyme is consistent with an interplay of factors including the capacity of the active site to bind large, negatively charged groups at the 6-position and overall oxidizability of each catecholamine, and is indicative of the utility of extradiol cleavage in semisynthetic and bioremediation applications.

# Introduction

Extradiol dioxygenase (EDX) chemistry is essential for catechol breakdown (Figure 1). The largest natural reservoir of catechols, 1,2-dihydroxybenzenes, is the plant woody-tissue polymer lignin. This polymer of catecholic monomers strengthens the cell

walls of a plant but impedes access to the cellusolic sugars used in biofuel production.<sup>1,2</sup> Lignin derived aromatic compounds are also an untapped source of carbon that could be valorized into feedstocks and natural products (Figure 1).<sup>3</sup> It is this utility of oxidative aromatic ring cleavage that has resulted in the adaptation of the extradiol cleavage reaction to the structural scaffolds of three distinct superfamilies – vicinal-oxygen-chelate (VOC), LigAB/PCAD, and cupin.<sup>4–7</sup> There are crystallographic examples from each superfamily, and in particular, for the VOC and cupin family EDXs, there are crystallographic and spectroscopic studies capturing and characterizing a variety of intermediates along the reaction pathway.<sup>8,9</sup>

The chemistry of extradiol dioxygenases was first exploited by nature to degrade the many monomeric lignin derived aromatic compounds, including hydroxylated benzoic acids such as gallate, O-methyl gallate, syringate and vanillate. The LigAB/PCAD superfamily enzymes responsible for this type of degradation are well-known for their promiscuity, and substrate specificities for members of this superfamily have been examined. For example, LigAB from Sphingomonas Paucimobilis SYK-6 can degrade 3,4-dihydroxybenzamide and 3,4-dihydroxybenzonitrile in addition to the traditional gallate, protocatechuate and basic catechol substrates. 5 Similarly, the LigAB/PCAD enzyme protocatechuate 2,3-dioxygenase from Bacillus macerans was observed to cleave 16 substrates in addition to the canonical protochatechuate, including chlorinated, nitrated and sulfonylated catecholic rings, albeit most with vastly reduced efficiency.8 While it does make lignin derived aromatic carbon more accessible, LigAB is promiscuous and prone to inactivation, requiring anaerobic purification for stable activity<sup>5</sup> and the product(s) of the enzymatic reaction have little biosynthetic utility. In contrast, VOC superfamily enzymes are believed to be somewhat less promiscuous and some members of this class are biosynthetic dioxygenases. For example, L-DOPA dioxygenase (NCBI CAA5574.1) is a member of the VOC superfamily. It is characterized by a distinct topology and domain organization. 9 and it is present in nature as a part of a biosynthetic pathway to the antibiotic lincomycin; taking the catechols of nature and recycling them into useful materials.

In part due to the paucity of synthetically available substrates, the wealth of VOC dioxygenases present in the databases are frequently annotated as no more than "biphenyl" or "catechol" dioxygenases after the founding extradiol dioxygenase members of this superfamily.<sup>10,11</sup> A handful of VOC family dioxygenases have been kinetically interrogated with respect to substrate tolerance, <sup>12–15</sup> but beyond the prototypical 2,3-dihydroxybiphenyl (2,3-DHB), homoprotocatechuic acid (HPCA, also known as 3,4-dihydroxyphenylacetic acid) or catechol, alternative substrates are mostly limited to methylated, chlorinated and sometimes nitrated catechols. The studies of activity for these alternative substrates either do not consider the co-substrate oxygen, <sup>14,15</sup> or the experiments consider O<sub>2</sub> but are ignorant of structure <sup>12</sup> or both. <sup>13</sup> Furthermore, these alternative substrates may have different electronic properties, but as these molecules are commercially available versus synthetically designed, they poorly approximate the native substrates, which complicates any understanding of electronic effects with questions of binding and steric effects within the substrate space.

Beyond this characterization of limited substrate tolerance among VOC superfamily dioxygenases, the study of the extradiol dioxygenase reaction mechanism itself is characterized by even less substrate diversity. The excellent work of Lipscomb and colleagues has defined mechanism and reaction intermediates for the VOC dioxygenase superfamily and is largely responsible for informing mechanistic understanding in the cupin and LigAB/PCAD dioxygenase superfamilies as well. This mechanistic study was accomplished largely through observations of the inhibitor/alternative substrate 4-nitrocatechol, a functionally limited analog of the native substrate HPCA, on the enzyme homoprotochatechuate-3,4-dioxygenase (HPCD). 14,16-18 Mechanistic work on the native, catecholic substrates for HPCD, 19,20 2,3-dihydroxybiphenyl -2,3-dioxygenase (DHBD)21,22 and catechol-2,3-dioxygenase also exist 23,24 and these studies have been essential for defining the intermediates that

currently describe the extradiol dioxygenase mechanism (Figure 2). However, the extent to which this mechanism applies across the VOC superfamily and beyond is limited by our understanding of that mechanism as it operates on a variety of substrates and across different superfamily members. For example, in addition to the limited suite of substrates examined for mechanism, the mechanistic work available in the VOC superfamily has only been performed on enzymes of form V topology <sup>9,25</sup> - enzymes which represent only a fraction of the EDX diversity within the VOC.

In an effort to expand our understanding of substrate diversity and mechanism across the VOC superfamily, we undertook the study of L-DOPA dioxygenase, a VOC dioxygenase of type IV topology<sup>9</sup> and performed a structurally-informed<sup>26</sup> examination of the cleavage reaction across a suite of electronically differentiated substrates, while considering oxygen as the co-substrate. Oxygen solubility and diffusion rate in aqueous solutions are poor, making the reactivity with oxygen an essential component of this study. Finally, the investigation of substrates and mechanism for L-DOPA dioxygenase has the added benefit of producing synthetically valuable dihydropyrroles/pyrrolines as products, converting lignin derived aromatic carbon into promising bio-synthons. The reactivity of dihydropyrroles/pyrrolines makes them desirable synthons in the preparation of more complex heterocycles.<sup>27,28</sup> This feature, in addition to the presence of L-DOPA dioxygenase and its homologs in natural product biosynthetic pathways to antibiotics and other bioactive molecules, 25 provides an interesting opportunity to exploit an understanding of these enzymes for semisynthesis. The anabolic role of these "biosynthetic dioxygenases" is full of potential if a study of steric and electronic features of substrate structure were implemented to deepen our understanding of catalysis. In fact, mutasynthesis and semisynthesis of natural products in this class have already shown promise. 29,30

To this end, we report herein the characterization of L-DOPA dioxygenase from S. lincolnensis as a ring-cleaving catalyst on a variety of 6-substituted dopamines. While L-DOPA (3,4-dihydroxyphenylalanine) is the native substrate of the enzyme, 3,4-dihydroxyphenethylamine (dopamine) is also a robust substrate (Figure 3). Given that 6-substitution of the dopamine ring was synthetically tractable<sup>31</sup> and the 3-substituted pyrroline produced from the oxidative cleavage of dopamine is a desirable synthon, we chose to investigate the steady-state kinetic parameters for a series of 6-substituted dopamines over a range of steric and electronic properties in order to interrogate the extent to which oxidation potential, catecholic pKa and substituent size/charge explain catalysis by the enzyme. Our results indicate that electron-withdrawing substituents are tolerated regardless of size, but that large, negatively charged substituents at the 6-position are poor substrates. The oxidizability of a substrate is consistent with its catecholic pKa values but is not a reliable predictor of ring cleaving potential Lastly, our results indicate that binding and reaction of molecular oxygen is impaired for all dopamine (DA) and 6-X-dopamine (6-X-DA) derivatives, and this is likely due to an extension of the the reaction pathway, possibly caused by additional space at the active site and a non-productive binding mode of oxygen. These findings not only have implications for predicting substrates of L-DOPA dioxygenase homologs within the VOC superfamily, they also impact our understanding of extradiol dioxygenase catalysis on alternative substrates more broadly.

# Results and Discussion

#### Synthesis and characterization of dopamine derivatives

Study of extradiol dioxygenase activity is frequently limited by the availability of sterically and electronically diverse substrates of the enzyme. 6-Substituted dopamine derivatives were designed and synthesized with a variety of electron-withdrawing substituents (Figure 3, S1).<sup>31</sup> The 6-position of the ring is not only synthetically accessible, it is also removed from the site of ring cleavage so as not to exert direct influence over the

bond-breaking steps. The effect of the 6-substituent was designed to be largely electronic<sup>31</sup> and significantly affect the deprotonation and oxidation potential of the substrate. We anticipated that these electron-withdrawing substituents should yield substrates that react more slowly with the enzyme. Existing studies on EDX mechanism predict that deprotonation of the catecholic oxygen at carbon-3 of the catecholic ring is an essential step of substrate binding, and precedes 1-electron oxidation of the ring to the semiquinone radical (Figure 2).<sup>10,32,33</sup> Indeed, the 1-electron oxidation of the substrate could explain the difficulty with which other EDX enzymes activate electron-deficient substrates like 4-nitrocatechol.<sup>10</sup> In order to better understand the extent to which deprotonation and/or oxidation were relevant to rates of enzymatic cleavage by L-DOPA dioxygenase, the redox potentials of 6-substituted dopamines were measured along with pKa values for acidic protons. The solution of the L-DOPA dioxygenase crystal structure<sup>26</sup> also allowed us to speculate on steric effects of the substituents via *in silico* docking experiments.

In terms of oxidation potential relative to the unsubstituted dopamine, all of the 6-substituted synthetic derivatives are more difficult to oxidize: 6-bromodopamine < 6-carboxydopamine < cyclic dopamine < 6-cyanodopamine and lastly, 6-nitrodopamine (Table 1). In contrast, 6-hydroxydopamine was very easily oxidized, auto-oxidizing readily in air to a dark red product. Despite literature reports of 6-hydroxydopamine stability in solutions containing ascorbate, 34 in our hands hydroxydopamine could only be handled under strict anaerobic conditions, and upon exposure to air, it auto-oxidized immediately (Figure S5). Due to this inherent instability, 6-hydroxydopamine was not investigated further. Lastly, 6-nitrodopamine was not oxidizable in the cyclic voltammetry experiment, consistent with the strong electron-withdrawing effects of the nitro substituent.

Consistent with the high oxidation potentials, 6-cyanodopamine and 6-nitrodopamine also had the lowest catecholic pKa values (Table 2), existing in solution as a significant percentage of catecholic monoanion likely deprotonated at the C3-OH. The presence of

the electron-withdrawing group at the 6-position has the predicted effect on the pKa values of the dopamine analogs. These pKa values correlate more strongly with the Hammett sigma para constant compared to the sigma meta constant (Figure S2), providing further evidence that it is the hydroxyl group (C3-OH) para to the substituent that is being deprotonated first. The second catechol OH deprotonation has a pKa above 9 for both 6-cyanodopamine and 6-nitrodopamine (Table 2). Previous work indicates that the deprotonation of the C3-OH catecholic proton follows binding of the substrate to the Fe<sup>II</sup>. <sup>20,21</sup> The relatively low pKa for the C3-OH in both 6-cyano- and 6-nitrodopamine could make additional deprotonation at C4-OH less favorable and also raise the oxidation potential. In contrast, catecholic pKas for cyclic, 6-carboxy- and 6-bromodopamine were above 8 and more consistent with dopamine and L-DOPA. <sup>35</sup>

Lastly, in silico docking of the substrates was examined in order to ascertain the steric accessibility of the active site to the different substituents. MM2 minimized structures of all six derivatives were examined in all relevant protonation states as dictated by pKa: +1 (a protonated amine), -1 (neutral amine and deprotonated C3-OH), and +1/-1 (a protonated amine and deprotonated C3-OH). Docking was performed using the L-DOPA dioxygenase structure from Streptomyces sclerotialus, a close homolog of the S. *lincolnensis* enzyme. 9,26 The Fe<sup>II</sup> charge at the active site and charges on the dopamine derivatives were computed with ANTECHAMBER<sup>36</sup> prior to using the structures in docking. Docks were assessed by comparison to the experimentally visualized L-DOPA substrate included in the S. sclerotialus L-DOPA dioxygenase structure and through measurement of contacts to the active site Fe<sup>II</sup> and the catalytic residues His74 and Tyr144.926 Dopamine is able to dock with distances to the Fe<sup>II</sup>, His74 and Tyr144 that are consistent with the native substrate, while 6-bromo- and 6-cyanodopamine dock with only slightly elongated Fe<sup>II</sup>-O3 distances (Figure S3). Less favorable docks were observed for 6-carboxydopamine and 6-nitrodopamine; these two compounds share a large, negatively charged substituent at the 6-position. The 6-position occupies a hydrophobic pocket comprised of Trp44 and Leu46 of one chain and Val140 from the second chain. Asp136 is also within 5 Angstroms of a substituent at the 6-position

(Figure S3). When the docking results are considered in aggregate, the data indicate that as the 6-X substituent gets larger and/or more charged, it causes the docking algorithm to pivot the 6-X group away from the hydrophobic pocket (Trp 44.A, Leu 46.A, Val 140.B) and consequently lengthen the Fe<sup>II</sup>-O3 contact. Hence, cyclic dopamine with no 6-X substituent has the shortest Fe<sup>II</sup>-O3 distance (2.5 Angstroms), while 6-nitrodopamine and 6-carboxydopamine have the longest (3.6-3.7 Angstroms). Cyanoand bromo are not charged, but they are larger substituents with electron density and have slightly elongated Fe<sup>II</sup>-O3 distances (2.7-2.8 Angstroms). In addition, the charged 6-carboxydopamine and 6-nitrodopamine could experience additional destructive interactions with the Asp136 carboxylate, which could also contribute to the lengthening of the C3-OH contacts. Taken together, these results complicate our analysis of a putative substrate. While 6-bromodopamine appears a likely candidate for cleavage by the enzyme, and 6-nitrodopamine appears disfavored in all contexts (oxidation, pKa and docking), the fate of a substrate like 6-carboxydopamine or cyclic dopamine is more difficult to predict. The fate of each substrate with L-DOPA dioxygenase was therefore evaluated in a series of aerobic and anaerobic kinetic experiments.

# 6-Bromo-, 6-carboxy- and 6-cyanodopamine as L-DOPA dioxygenase substrates

In order to assess the activity of L-DOPA dioxygenase on dopamine and its 6-substituted derivatives, the aerobic, enzymatic reaction was observed by UV-Visible spectroscopy and the products of the enzymatic reaction analyzed by electrospray ionization - mass spectrometry. The extradiol cleavage of dopamine produces a bright yellow semialdehyde that is readily visualized. When a product was observed, the enzymatic reaction was interrogated with steady-state kinetic methods as a means for comparing substrates.

Initial assessment placed the compounds into two broad categories: 1) molecules that reacted with the enzyme in multiple turnovers and 2) molecules that were poor

substrates. Dopamine, 6-bromodopamine, 6-carboxydopamine and 6-cyanodopamine exhibited robust turnover and steady state kinetics of both the catecholic and oxygen substrates were measured (Tables 3 and 4, Figures S5, S6, S7, and S9). In comparison, cyclic dopamine and 6-nitrodopamine were poor substrates and will be discussed in the subsequent section.

Dopamine, 6-cyanodopamine, 6-carboxydopamine and 6-bromodopamine each produced a unique steady-state product that was identified as the respective CHAP (Figure 3) by MS (Figure S5 and S6). The extinction coefficient for each of these steady-state, cyclized products was determined at  $\lambda_{\text{max}}$  (Table 3) and dopamine and each derivative were then examined under conditions that varied substrate concentration (Table 4, Figure S7). Experiments which varied substrate concentration under air-saturated (21% O<sub>2</sub>) or oxygen-saturated (100% O<sub>2</sub>) conditions were modeled using Kintek Explorer and best described by a combination of substrate and product inhibition modifying a basic steady-state model (Figure S7). For each of these four substrates, as the substrate concentration was increased, the reaction showed marked inhibition, and this inhibition was not explainable by substrate decomposition or enzyme inactivation. Instead, modeling the data required both substrate and product inhibition terms. Fitting to this simple steady-state model (i) as described in Materials and Methods allowed for the determination of  $K_M$  and  $k_{cat}$  for each substrate along with rates to describe both the substrate and product inhibition terms. As shown in Table 3, if we compare experiments conducted at maximum O<sub>2</sub> saturation, the lowest K<sub>M</sub> belongs to dopamine and 6-bromodopamine, followed by a two-fold increase to the 6-cyanodopamine  $K_M$ , and lastly a thirty-fold increase to the  $K_M$  of 6-carboxydopamine. The k<sub>cat</sub> terms follow a similar pattern, where the fastest k<sub>cat</sub> at 8.7 s<sup>-1</sup> belongs to dopamine, followed by a seven-fold decrease in k<sub>cat</sub> for 6-bromodopamine and a nine-fold decrease for 6-cyanodopamine. Lastly, 6-carboxydopamine has the weakest k<sub>cat</sub> at an eleven-fold decrease from dopamine. That dopamine should be the best substrate followed by 6-bromodopamine was not surprising. 6-Bromodopamine exhibited an oxidation potential and pKa that were most similar to dopamine, and in

silico docking experiments predicted a reasonable substrate binding position, albeit with an elongated Fe<sup>II</sup>-O3 bond compared to the native substrate, L-DOPA and dopamine. However, the most telling observations were from the following comparisons: 1) 6-cyanodopamine is a better substrate by  $K_M$  (14-fold) and  $k_{cat}$  (1.3-fold) than 6-carboxydopamine. These data imply that binding of 6-carboxydopamine and the problems caused by a large, negatively charged 6-X-substituent outweigh the challenges in oxidizing a more electron deficient substrate like 6-cyanodopamine. 2) The substrate and product inhibition terms across the four substrates do not vary significantly; the inhibition is modest but persistent. However, the substrate and product inhibition terms worsen when comparing 100% O<sub>2</sub> saturation to experiments for dopamine and 6-cyanodopamine at air (21%  $O_2$ ) saturation. In addition, the  $K_M$  and  $k_{cat}$ for both dopamine and 6-cyanodopamine get larger and slower. For dopamine, the K<sub>M</sub> increases by nearly five-fold, and the k<sub>cat</sub> slows by nearly six-fold when the oxygen concentration during the experiment decreases from 100% O<sub>2</sub> saturation to 21% O<sub>2</sub>/air saturation. Similarly for 6-cyanodopamine, the K<sub>M</sub> increases and the k<sub>cat</sub> slows by almost two-fold as the oxygen concentration decreases from 100% to 21%. These observations strongly implied that insufficient oxygen concentration was contributing to the steady-state inhibition terms. 3) Lastly, K<sub>M</sub> and k<sub>cat</sub> for L-DOPA, the native substrate, are not complicated by any substrate and product inhibition terms; furthermore, the steady-state constants are more consistent from 21% O<sub>2</sub> to 100% O<sub>2</sub> saturation. For L-DOPA,  $K_M$  at 21%  $O_2$  increases by only 1.3-fold and the  $k_{cat}$  is constant within error.

Oxygen is a co-substrate of the L-DOPA dioxygenase reaction (Figures 2 & 3). In order to understand the effects of oxygen concentration on the reaction, the steady-state kinetics of the L-DOPA dioxygenase reaction were examined for each of the four active dopamine substrates: Dopamine, 6-bromodoapmine, 6-cyanodopamine and 6-carboxydopamine, while varying oxygen concentration. These experiments were inherently limited by the maximum concentration of dissolved oxygen at the temperature of the experiment. For example at 22°C, saturation of the buffer with 100% O<sub>2</sub> yields a maximum concentration of 1.2-1.3 mM O<sub>2</sub>. There were further limitations when it came

to 6-carboxydopamine. Ideally, measuring steady state kinetics for  $O_2$  requires that the second substrate, in this case the dopamine/6-X-DA, must be in 5-10-fold excess of the  $K_M$ , but the  $K_M$  for 6-carboxydopamine was so high (~3.8 mM), that limitations on solubility and availability meant that higher concentrations simply could not be achieved. In this instance, we opted to run the steady-state kinetic experiments to vary oxygen at a " $K_M$ " concentration of 6-carboxydopamine. For internal comparison, a similar experiment was conducted for dopamine and 6-bromodopamine. The results of the steady-state kinetics to vary oxygen are represented in Table 3 and Figure S9. The most obvious conclusion is that the  $K_M$  for  $O_2$  is markedly increased for dopamine, as well as 6-bromodopamine, 6-cyanodopamine and 6-carboxydopamine when compared to the native substrate L-DOPA.

The natural substrate L-DOPA has such a tight K<sub>M</sub> O<sub>2</sub>, that we were only able to estimate an upper limit. At saturating L-DOPA concentrations, the K<sub>M</sub> O<sub>2</sub> was estimated at ~3 µM (or ~0.2% oxygen), but the large uncertainty in this number is a function of the experimental difficulty in getting oxygen concentrations below 21%/air-saturation. Reducing the L-DOPA concentration to 3x the L-DOPA K<sub>M</sub> allows for an estimate of an upper limit for the K<sub>M</sub> O<sub>2</sub> when L-DOPA is substrate of 53.2 ±1.6 μM or ~4% oxygen at 22°C; well below the concentration of oxygen in a room-temperature, air-saturated solution. In contrast, when saturated with dopamine substrate, at a concentration that minimized substrate inhibition, the  $K_M$   $O_2$  was 499  $\pm$  31  $\mu$ M, easily a ten-fold increase in oxygen K<sub>M</sub> when compared to the native L-DOPA substrate. Furthermore, in fitting these data, an alternative derivation of the Michaelis-Menten expression was used in which  $k_{cat}$  and  $k_{cat}/K_M$ , also known as  $k_{SP}$  are derived directly from the fitting and  $K_M$  is determined from the two fitted constants  $(K_M = k_{cat}/k_{SP})$ . Under conditions where L-DOPA, dopamine or 6-X-DA is saturating,  $k_{SP}$  or  $k_{cat}/k_{M}$  is the second order rate constant for the reaction of oxygen with the enzyme. As shown in Table 3, this second order rate constant is four- to ten-fold slower with DA and 6-X-DA when compared to the native substrate L-DOPA.

Based on the K<sub>M,DA/6-X-DA</sub>,  $k_{cat}$  and  $K_{M,O2}$  and  $k_{SP,O2}$  measurements, the overall pattern of reactivity for the four active DA/6-X-DA substrates was 6-bromodopamine > dopamine > 6-cyanodopamine > 6-carboxydopamine. This pattern is consistent with several competing factors: 1) dopamine and 6-bromodopamine are the easiest to oxidize and can adopt native substrate-like positions in the active site, so it is reasonable that these are best substrates. 6-Bromodoamine is somewhat more difficult to oxidize than dopamine, which may explain the lower k<sub>cat</sub> but the K<sub>M</sub> O<sub>2</sub> and k<sub>SP</sub> O<sub>2</sub> for 6-bromodopamine are ten-fold improved over dopamine, which may indicate that the larger 6-bromodopamine substrate is more compatible with effective reaction with oxygen; 2) 6-cyanodopamine is difficult to oxidize (Table 1) but adopts a much more favorable geometry in the active site (Figure S3); 3) 6-carboxydopamine is more difficult to oxidize than 6-bromodopamine, but not as difficult as 6-cyanodopamine; however, it adopts an unfavorable geometry at the active site due to its large, negatively charged substituent. Taken together, these results imply that active site position is more important than inherent oxidizability, and that an elongated Fe<sup>II</sup>-O3 bond, as was observed in docking experiments, may compromise the effective binding of oxygen and subsequent interaction with the DA/6-X-DA substrate. In the case of 6-bromodopamine, this molecule seems to occupy an ideal position, both oxidizable enough and the right size and charge to facilitate effective catalysis.

Lastly, these steady state kinetic data imply that the binding and reaction of oxygen with the dopamine/6-X-DA substrate is compromised relative to the native system of L-DOPA. The inherent limitations on the amount of oxygen that can be dissolved in a solution at a given temperature dictated that oxygen was not saturating in our experiments to vary DA/6-X-DA, and likely created the appearance of substrate and product inhibition as the DA/6-X-DA concentration was increased. This behavior is absent in the native L-DOPA reaction. What is less obvious is why the simple removal of a single carboxylic acid group from the side chain of L-DOPA, which is the only difference between L-DOPA and dopamine, should have such a significant impact on the enzymatic reaction in this way. These observations led us to conclude that it might

be possible to observe these perturbations in oxygen binding and catalysis if the enzymatic reaction were observed in the pre-steady state (see *Pre-steady state evaluation of dopamine cleavage*).

# 6-Nitrodopamine and cyclic dopamine as L-DOPA dioxygenase substrates

Under initial examination, cyclic dopamine and 6-nitrodopamine did not exhibit multiple turnovers amenable to steady-state kinetics. Docking experiments predicted active site binding was compromised but possible for both 6-nitrodopamine and cyclic dopamine (Figure S3); furthermore, these are two of the three most difficult substrates to oxidize (Table 1). In order to determine if these molecules were binding to the active site at all, the substrates were examined anaerobically for binding and formation of the catecholate (Figure 2). As shown in Figure 2, when the substrate binds to the active site Fe<sup>II</sup>, a proton is lost to form the asymmetric chelate. In the case of 6-nitrodopamine, the first catecholic pKa at 6.3 is attributed to the loss of C3-OH (Table 2); however, the enzyme should remove C4-OH, to generate a dianion at  $\lambda_{max}$  510 nm. Indeed, in the presence of the enzyme, and in the absence of oxygen the 510 nm dianion appears with an isosbestic point at 452 nm connecting it to the 420 nm starting peak of the 6-nitrodopamine monoanion (Figure S10). Oxygen electrode and UV-Visible spectroscopy data agree that 6-nitrodopamine completes less than one full turnover, but it is possible to detect formation of products by MS (Figure S5).

The oxidation potential of free cyclic dopamine was very similar to 6-carboxydopamine and 6-bromodopamine (Table 1). This correlation was initially surprising to us, since the cyclic dopamine has a pKa (Table 2) and Hammett constant<sup>31</sup> (Figure S2) consistent with a more electron-rich catechol; however, the cyclic dopamine proved to be a difficult substrate for L-DOPA dioxygenase, and completed less than one full turnover (Figure S10). While we predict that cyclic dopamine is able to access the active site Fe<sup>II</sup> and adopt a reasonable geometry, it is likely that the higher-than-expected oxidation

potential is a reflection of the rigid bicyclic cyclic dopamine structure, a feature that likely makes enzyme-catalyzed ring cleavage all but impossible. Oxidation of the catecholic ring is expected to produce a semiquinone, and observations of a comparable semiguinone in the structure of 2,3-HPCD<sup>17</sup> indicate the ring is bent out of the plane. Cyclic dopamine would experience greater torsional strain from ring puckering due to semiguinone formation, which may explain why the oxidation potential is higher than expected for the free molecule in solution, and why enzymatic activity on this substrate is weak. Cyclic dopamine is able to in silico dock at the active site with Fe-O distances (O3-Fe<sup>II</sup> 2.50 Å, O4-Fe<sup>II</sup> 2.29 Å) that approximate those of the native substrate observed in the crystal structure (O3-Fe<sup>II</sup> 2.53 Å, O4-Fe<sup>II</sup> 2.47 Å), but at 3.19 Å the O3-Tyr distance in the cyclic dopamine dock is 16% longer than the same distance in the experimental substrate. In homologous VOC dioxygenases, the active site tyrosine has been implicated in oxygen-activation and catalysis through interactions with the nearby catecholic O-H (C3-OH for dopamine); 17,20 the same C3-OH that is deprotonated by the enzyme. The greater distance between the C3-OH and the Tyr-OH (Tyr139 in S. lincolnensis) could indicate that the cyclic dopamine substrate is also poorly positioned for substrate activation. This is consistent with a weak formation of the catecholate as seen in Figure S10.

### Pre-steady state evaluation of dopamine cleavage

Steady-state characterization of dopamine and synthetic dopamine derivatives revealed impaired oxygen binding relative to wild-type substrate L-DOPA. The weaker  $K_M O_2$  (Table 3) is consistent with difficulty in achieving saturation of the enzyme by oxygen, and is likely what also contributed to the observation of inhibition kinetics in the steady state. These steady-state implications of impaired catalysis with respect to oxygen were surprising, given the relative structural similarity between L-DOPA and dopamine, and the ease with which docking experiments predict dopamine binding to the active site. These observations led us to examine the reaction in the pre-steady state for additional evidence of impaired catalysis with respect to oxygen binding.

As shown in Figure 2, oxygen binding is followed by oxidation of the substrate to the radical semiquinone via the active site Fe<sup>II</sup>. The semiquinone of L-DOPA and of dopamine have known absorbance spectra;<sup>38,39</sup> however, examination of the L-DOPA reaction in the pre-steady state has no features consistent with the appearance of a semiquinone.<sup>9,40</sup> Presumably, in the reaction of L-DOPA, the semiquinone forms and decays so rapidly that any spectroscopic features are lost in the mixing time. But, if oxygen binding and subsequent reaction steps are slowed in the reaction of dopamine, then a semiquinone might be visible. Indeed, a similar experiment was performed on the Y257 mutant of homoprotocatechuate-2,3-dioxygenase (HPCD).<sup>20</sup> This HPCD mutant is also impaired in oxygen activation (Y257 is the active site tyrosine of HPCD that is represented in Figure 2), and pre-steady state evaluation of the reaction was consistent with the accumulation of a semiquinone of the HPCD substrate.

The reaction of dopamine with L-DOPA dioxygenase was examined in the pre-steady state under single and multiple turnover conditions. The inherent limitation of oxygen solubility in buffer and the impaired oxygen binding in the presence of dopamine (Table 3) meant that truly saturating oxygen concentrations for the dopamine substrate were not achievable; however, despite these limitations, it was possible to see an early spectroscopic feature appearing and disappearing within the first second of the reaction when the reaction was observed at 360 nm. The wavelength 360 nm was chosen because it is between the wavelength maximum of the initial enzymatic product of dopamine cleavage (375 nm for AEHMS, *data not shown*) and the wavelength of maximum absorbance for the dopamine semiquinone, and the data were modeled to a reaction pathway based on Figure 2 as described in the Materials and Methods. The dopamine semiquinone has been independently observed and characterized with absorption maxima at 309 and 340 nm. <sup>38,39</sup> In addition, the cyclized cleavage product of dopamine (CHAP, Figure 3) also has a small amount of absorbance at 360 nm (5,280 ± 30 M<sup>-1</sup> cm<sup>-1</sup>, Figure S8).

In modeling the L-DOPA dioxygenase reaction with dopamine, the first apparent conclusion was that the feature appearing and disappearing within the first second (Figure 4A) was consistent with a model in which a semiquinone species appears before Fe-alkylperoxo formation (Figure 2) breaks the ring aromaticity, and the UV-visible signal at longer wavelengths is lost until ring cleavage of "the lactone" (Figure 2) reestablishes the continuous sp² character and the long-wavelength UV-Visible absorbance of the semialdehyde product. The data trace in Figure 4A was fit to a model that predicts transient accumulation of a semiquinone. Because it was independently determined (Figure S8), the extinction coefficient of CHAP at 360 nm was fixed during fitting. Constraining the predicting rates also required fixing the extinction coefficient for AEHMS at a reasonable value ( $\varepsilon_{360} \sim 34,000 \text{ M}^{-1}\text{cm}^{-1}$ ), but the fitting of the data was capable of predicting an extinction coefficient for the semiquinone (ESQ) of 3,075 ± 695 M<sup>-1</sup>cm<sup>-1</sup>.

Close examination of the first few milliseconds of the dopamine trace (Figure 4A) revealed a faster rate preceding formation of the apparent semiquinone, but there were insufficient data points (so soon after mixing) to fit this rate reliably. In addition, observations of anaerobic enzyme substrate binding for 6-cyanodopamine indicated that this derivative dopamine substrate bound to the enzyme over a minimum of two steps (Figure S11); that is, a minimum of two steps preceded oxygen binding. 6-Cyanodopamine has a chromophore and is fluorescent, so it was amenable to anaerobic binding experiments where dopamine is not. To accommodate these observations,  $k_1$  and  $k_2$  were included in the model as steps preceding the binding of oxygen. The rates  $k_1$  and  $k_2$  were fixed as shown in Figure 4, while  $k_2$  was computed by fit to the data ( $k_{\cdot 2}/k_2$  fixed at 10  $\mu$ M) to enable fitting of the subsequent spectroscopic feature assigned to the semiquinone. Without  $k_1$  and  $k_2/k_2$ , the semiquinone appeared too early in the reaction trace.

The second conclusion came from concentration dependent experiments with dopamine substrate. When performing concentration dependent experiments of dopamine with the

enzyme (Figure 4C), the relative amplitudes of the traces were unexpectedly close, as though the increase in concentration of substrate did not produce a commensurate increase in activity. This was in obvious contrast to existing data on the L-DOPA substrate from our laboratory, 9,40 in which concentration dependent experiments on the L-DOPA substrate produced traces with amplitudes that increased proportionally to the substrate concentration. This behavior was oddly reminiscent of the steady-state data, in which increasing concentrations of substrate produced apparent inhibition (Table 4, Figure S7). Not only did this phenomenon persist across temperature, concentration range, and wavelength of observation (data not shown), the behavior could not be explained by modeling enzyme inactivation over the course of the experiment or by modeling the accumulation of an inhibitory species from side reactions of the substrate. In the end, the behavior was best explained by the comprehensive model shown in Figure 4E, in which the binding of oxygen and electron transfer to produce the semiquinone has the option to travel a longer kinetic path in which the semiquinone is not compatible with Fe-alkylperoxo formation; we named this species ESQ X (Figure 4) and fit the rate of formation and decay of ESO\_X (k<sub>6</sub> and k<sub>-6</sub>) using the concentration dependent data in Figure 4C. In one sense, the formation of ESQ X is a type of "inhibition" in which oxygen binding produces an intermediate that is not compatible with forward reaction, and in effect, the reaction stalls and inhibition is apparent. It is also possible to interpret these data as evidence for multiple binding modes for oxygen; only a subset of which is compatible with Fe-alkylperoxo formation and forward reaction to product. This interpretation is furthermore consistent with existing data on oxygen-binding and intermediate formation at the active site of extradiol dioxygenases. For example, oxygen has been observed in a side-on (Figure 2) orientation at the active-site iron in crystal structures of HPCD with nitrocatechol, 17 while end-on binding of the oxygen mimic NO was observed for the same enzyme in another instance.41 Recently, end-on oxygen binding was also observed in crystal structures of the cupin extradiol dioxygenase 3-hydroxyanthranilate-3.4-dioxygenase<sup>33</sup> and end-on versus side-on binding of oxygen has been a source of some controversy in the study of other

extradiol dioxygenase enzymes. <sup>42</sup> Taken together, these studies demonstrate that different binding modes of oxygen binding are possible at the non-heme Fe<sup>II</sup> active site common to EDX enzymes, but neither do they preclude the possibility that one mode of oxygen binding is more catalytically competent over another. Our data raise the possibility that progress to Fe-alkylperoxo formation from the semiquinone (Figure 2) could be inhibited by a non-productive binding mode of oxygen and subsequently, the superoxide species that must form a bond with C3 of the substrate. It is plausible to speculate that the absence of the carboxylate functional group from the side chain of dopamine, the only structural difference between dopamine and L-DOPA, creates additional space at the active site. The active site is already well solvated<sup>26</sup> and the additional space could create the opportunity for oxygen to sample a variety of binding modes of varying catalytic competency.

Our model also predicts that the inhibitory complex (ESQ\_X) can reform a catalytically competent superoxide-semiquinone complex (ESQ) and go on to form product. This is also consistent with the theory in which the inhibition is observed from non-productive binding modes of oxygen. The Figure 4D model was designed to be complementary between the literature consensus on dioxygenase mechanism (Figure 2) and what these kinetic data could illuminate; therefore, there are steps in the reaction pathway for which intermediates have been observed by others, but are not visible by the spectroscopic methods used herein. Steps between the Fe-alkylperoxo and the semialdehyde product (EI1 to EI3) including the lactone (Figure 2) are not expected to have long-wavelength UV signatures owing to the sp³ interruption of conjugation. Therefore, intermediates after the semiquinone (ESQ) were included in the model shown in Figure 4, but the rates of formation were fixed at values fast enough not to impact the species observed.

# Conclusions

Extradiol dioxygenase enzymes have enormous catabolic and biosynthetic potential to recycle and repurpose lignin derived aromatic carbon into useful materials. However,

this potential is limited by what we don't know about substrate space and flexibility in catalysis. This challenge can only be addressed by the study of a variety of substrate structures synthetically tailored to address questions of size, electronics, and ultimately, mechanism within the context of active site structure and alongside the co-substrate, oxygen.

In this study, we have demonstrated that L-DOPA dioxygenase is competent to cleave dopamine analogs with steric and electronic diversity. In the case of electron rich, but neutral substituents like 6-bromo- and 6-cyanodopamine, the better substrate was the molecule that was more easily oxidized, but effective catalysis with oxygen was influenced by substituent size. Secondly, the cost of binding a large, negatively charged substituent at the 6-position outweighs the challenge of oxidation potential in the case of 6-carboxydopamine versus 6-cyanodopamine. Lastly, 6-nitrodopamine was still a weak substrate despite its unfavorable oxidation potential and large, negatively charged substituent.

When comparing dopamine to 6-bromodopamine, the two molecules are very competitive substrates. Most strikingly, 6-bromodopamine has oxygen dependent kinetics that are most comparable to L-DOPA. Again, these results challenge the prevailing assumption that oxidation potential dictates the effectiveness of dioxygenase substrates of similar size. 6-Bromodopamine is more difficult to oxidize than dopamine, but it is also larger, and the neutral substituent at the 6-position does not interact unfavorably with the hydrophobic pocket and with Asp136 (Figure S3). Furthermore, the larger 6-position substituent may in-part compensate for the extra room created at the active site from the missing carboxylic acid of L-DOPA and may limit the non-productive binding modes of oxygen implied by pre-steady state kinetic data. As shown in Table 3, the entire class of dopamine derivatives was typified by poor oxygen  $K_M$  and a weaker  $k_{SP}$  relative to the reaction of  $O_2$  with the native substrate L-DOPA. And when the reaction of L-DOPA dioxygenase with dopamine was examined more closely, pre-steady state kinetics indicated that oxygen may be binding and oxidizing the substrate to a

semiquinone, but in a binding mode that is not productive for further reaction. Our model predicts that this non-productive mode of oxygen binding and activation is plausibly what partially stalls the progress of the reaction and gives the appearance of inhibition.

Indeed, these conclusions connect to and are supported by observations that existed within the literature prior to this study. Furthermore, this work not only builds upon but unites previous experimentation on extradiol dioxygenases, substrate specificity and mechanism. Study of extradiol dioxygenase mechanism has been limited to a small subset of catecholic substrate analogs and studies of substrate specificity that have attempted to inform mechanism have either ignored structure or the co-substrate oxygen or both. However, if we take into account the assertions made herein regarding the co-substrate oxygen and the non-productive binding modes implied by pre-steady state experiments, it is possible to reconcile these data with what already exists in the literature.

Firstly, it is not possible to explain the substrate specificities examined herein without invoking competition between substituent size, substituent charge and oxidation potential. The same conclusions were drawn in the analysis of LigAB with alternative substrates. The structural homogeneity of our substrate suite further emphasizes this conclusion. Secondly, the K<sub>M</sub> for oxygen is an essential component of these interpretations, and others have made the same observations. But in these cases: catechol-2,3-dioxygenase<sup>12</sup> and DHBD, <sup>15</sup> the K<sub>M</sub> for oxygen is very high for the "native" substrate, so high that oxygen cannot be saturating under conditions where the catecholic substrate is varied. In the case of the VOC enzyme catechol 2,3-dioxygenase, the authors measure the second order rate for oxygen (k<sub>cat</sub>/K<sub>M,O2</sub> which is equivalent to a k<sub>SP</sub> for oxygen) and conclude that increasing the electron-withdrawing nature of the substituent is compromising oxygen binding and catalysis. This is consistent with our theory of non-productive oxygen binding in the case of misaligned or difficult-to-oxidize substrates. In addition, the low K<sub>M</sub> O<sub>2</sub> and absence of substrate inhibition for L-DOPA dioxygenase with its native substrate L-DOPA is an interesting

contrast to an enzyme like DHBD with the "native" substrate, 2,3-DHB. Substrate inhibition and substrate-based inactivation in extradiol dioxygenase enzymes may be more broadly symptomatic of ineffective catalysis with oxygen due to space at the active site for non-productive binding modes for oxygen, and possibly substrate as well.

An extension of this reasoning can also be applied to the VOC extradiol dioxygenase, DHBD which acts on 2,3-dihydroxybiphenyl (DHB) as its "native" substrate. The  $K_{MO2}$  for DHBD is very high (four times the concentration of oxygen in air saturated buffer), and interestingly, the enzyme exhibits substrate inhibition with DHB. 15 While the authors do not consider oxygen binding in the context of the alternative substrates, they do examine enzymatic inactivation as a function of substrate; a process which is oxygen dependent. Briefly, the enzyme activates oxygen generating semiquinone intermediate and superoxide, but the superoxide disassociates and the enzyme is inactivated.<sup>22</sup> This rate of inactivation is increased with the use of alternative substrates like catechol, which are substantially smaller than DHB. 15 The rate of inactivation, an oxygen dependent process that presumably generates a semiguinone intermediate, alongside the substrate inhibition for DHB can both be explicated by our interpretation of active-site space creating non-productive oxygen binding modes that stall the reaction and result in apparent "substrate inhibition". This is also a plausible explanation for the "substrate inhibition" observed for other single-domain BhpC enzymes13 when the smaller catechol is used as an alternative substrate.

HPCD is also a VOC extradiol dioxygenase of the same sub-type as DHBD and catechol-2,3-dioxygenase, and the use of alternative substrates 4-nitrocatechol and 4-sulfonylcatechol result in higher rates of inactivation despite crystallographic evidence that substrate binding is competent for catalysis.<sup>14</sup> These data can also be understood within the same framework. The crystallographic evidence does not consider the binding of oxygen, but the alternative substrates used seem to allow for more room at the active site, such that a new water molecule appears in the active-site model.<sup>14</sup> In this instance, contributions to catalytic breakdown from non-productive oxygen binding

modes, made permissible by additional space at the active site, could contribute to the increased rate of inactivation, despite the evidence of steric compatibility. Finally, this increased rate of inactivation is also observed for LigAB (a type 2, PCAD superfamily enzyme) in the presence of alternative substrates,<sup>5</sup> implying that the compromised oxygen catalysis in the presence of alternative substrates is likely a phenomenon that occurs for extradiol dioxygenases regardless of superfamily.

In completing this work, our goal was to inform the study of extradiol dioxygenase chemistry in a way that looks beyond one corner of the VOC superfamily and helps to explain catalysis more broadly within and across substrate space. And with the results presented herein, we have provided an organizing theory that unites previous understanding while enriching and illuminating our understanding of substrate specificity in extradiol dioxygenase enzymes. Substituent size and charge do matter to the extent that each interrupts effective reaction with activated oxygen, and oxidation potential of the substrate is less important. Lastly these results unequivocally demonstrate that it is important to address impacts to oxygen binding and reaction in the cleavage of non-native substrates when considering EDX enzymes more broadly as catalysts for bioremediation or semisynthesis.

#### Materials and Methods

#### Small-molecule Docking

The *S. sclerotialus* L-DOPA dioxygenase holo structure<sup>26</sup> (PDB: 6ON3) was modified by isolating one dimer and deleting L-DOPA from the active site. Substrate structures were drawn, MM2 energy-minimized, and manually adjusted to reflect standard bond lengths using Chem3D. Formal charges were assigned using Chem3D, and atomic partial charges were computed using the AM1-BCC method.<sup>36</sup> The presence of solvent molecules in the dock was controlled via the dock prep function, and each dock was

performed with and without water molecules. The receptor and ligand structures were prepared using the dock prep function in UCSF Chimera.<sup>43</sup>

Ligand structures were docked into the active site of L-DOPA dioxygenase using AutoDock Vina version 1.1.2.<sup>44</sup> The search volume was centered on the ligand binding site using grid box dimensions of 12.8 Å x 9.5 Å x 11.0 Å. Net charges of -1, 0, and +1 were applied to each dopamine derivative using the AM1-BCC method.<sup>36</sup> Triplicate docks subjected to the following parameters were executed to ensure consistency of docking results: hydrogens were added when appropriate, charges were merged, non-polar hydrogens and lone pairs were removed, water molecules were ignored, and chains of non-standard residues were ignored. Docks were qualitatively evaluated by their scores and by pose similarity to the natural orientation of L-DOPA in the published crystal structure. Docks were quantitatively evaluated by measuring the distances from the catecholic oxygens of the ligand to the Fe<sup>II</sup>, Y144 (chain B), and H74 (chain A).

#### Cyclic Voltammetry of dopamine and 6-substituted derivatives

Electrochemical evaluation was performed in accordance with Silva, et. al. at physiological pH 7.4 by cyclic voltammetry (CV).  $^{45,46}$  Voltammetric measurements were performed using an CH Instruments 600E potentiostat in a one-compartment cell equipped with a three-electrode system arrangement composed of a platinum wire as auxiliary electrode, a saturated calomel electrode as reference, and a glassy carbon electrode (GCE, d = 2 mm) as working electrode. All measurements were conducted at room temperature (25 ± 1°C) and purified nitrogen was used for oxygen displacement. The working electrode was polished manually between each scan with an aqueous slurry of alumina powder on a microcloth pad and rinsed with water before use. Each sample contained 0.1 mM substrate 0.1 M phosphate buffer (pH = 7.4), 1  $\mu$ M DMSO in a volume of 5 mL.

### Synthesis of 6-bromodopamine (6-bromoDA)

Unless otherwise indicated, all anhydrous solvents were commercially obtained and stored in Sure-Seal bottles under argon. All other reagents and solvents were purchased as the highest grade available from Acros or Sigma-Aldrich and were used without further purification. All moisture-sensitive reactions were carried out using dry solvents and under slight pressure of ultra-pure argon. Commercially available disposable syringes were used for transferring reagents and solvents. All single syntheses were conducted in conventional flasks under an atmosphere of dry argon. Proton (¹H) and carbon (¹³C) NMR spectra were recorded on a Varian 400 MHz spectrometer. Chemical shifts (δ) are reported in parts per million (ppm) referenced to ¹H (CHCl₃ at 7.26, CH₃OH at 3.31), ¹³C (CDCl₃ at 77.16, CD₃OD at 49.15). Coupling constants (*J*) are reported in Hz throughout. Column chromatography was conducted using silica gel (Silicycle 55-65 Å). Compound **2** was prepared from 3,4-dimethoxyphenethylamine as previously described.³¹

## N-(2-bromo-4,5-dimethoxyphenethyl)acetamide

Compound **2** (1.017 g, 3.58 mmol, 1 eq.) and acetic acid (14.5 mL) was added to round-bottom flask and stirred at rt under Ar. A solution of  $Br_2$  (0.25 mL, 3.58 mmol, 1 eq.) and acetic acid (0.5 mL) was added dropwise at rt; the reaction was stirred for 3 h at which time the reaction mixture was diluted with  $CH_2CI_2$  (30 mL) and washed with sat.

Na<sub>2</sub>S<sub>2</sub>O<sub>3</sub> solution (15 mL). The organic layer was removed and the aqueous layer was washed with an additional portion of  $CH_2CI_2$  (10mL). The organic layers were combined and were washed with brine before being dried with Na<sub>2</sub>SO<sub>4</sub> and concentrated *in vacuo*. The crude product was purified by silica gel column chromatography (98:2  $CH_2CI_2/CH_3OH$ ) to afford compound **3** as a white powder (1.03 g 95.4%). **R**<sub>f</sub> (9:1  $CH_2CI_2/CH_3OH$ ): 0.459. <sup>1</sup>**H NMR** (400 MHz,  $CDCI_3$ ):  $\delta$  7.01 (s, 1H), 6.73 (s, 1H), 5.56 (s, 1H), 3.86 (s, 3H), 3.85 (s, 4H), 3.49 (t, 1H), 2.90 (t, J = 7.0 Hz, 2H), 1.97 (s, 3H). <sup>13</sup>**C NMR** (101 MHz,  $CDCI_3$ ):  $\delta$  148.55, 148.36, 130.06, 115.57, 114.19, 113.34, 77.32, 77.00, 76.68, 56.17, 56.13, 39.76, 35.28, 23.20.

#### tert-butyl acetyl(2-bromo-4,5-dimethoxyphenethyl)carbamate

Compound **3** (493 mg, 1.65 mmol, 1 eq.), 4-dimethylaminopyridine (204 mg, 1.65 mmol, 1 eq.), and anhydrous acetonitrile (12 mL) were added to a round bottom flask under Ar at rt. Di-*tert*-butyl dicarbonate (750 mg, 3.40 mmol, 2 eq.) was dissolved in anhydrous acetonitrile (2 mL) under Ar and added to the reaction mixture. The solution was stirred overnight at rt. The resulting solution was diluted with EtOAc (15 mL) and the organic layer was washed with a sat. NH<sub>4</sub>Cl solution (20 mL x 3). The crude product was concentrated *in vacuo* and then purified by a silica gel column chromatography (95:5  $CH_2CI_2/MeOH$ ) to afford compound **4** as a pale, yellow flake (456 mg 68.7%). **R**<sub>f</sub> (9:1  $CH_2CI_2/CH_3OH$ ): 0.886. <sup>1</sup>**H NMR** (400 MHz,  $CDCI_3$ ):  $\delta$  6.99 (s, 1H), 6.70 (s, 1H), 3.91 (t, 3H), 3.84 (s, 5H), 3.84 (s, 2H), 2.91 (t, 3H), 2.48 (s, 3H), 1.48 – 1.41 (m, 11H). <sup>13</sup>**C NMR** (101 MHz,  $CDCI_3$ ):  $\delta$  173.15, 153.11, 148.44, 148.28, 130.49, 115.45, 114.29, 113.58, 82.96, 77.32, 77.00, 76.68, 56.18, 56.03, 44.22, 34.56, 27.94, 27.88, 27.00.

#### tert-butyl (2-bromo-4,5-dimethoxyphenethyl)carbamate

Compound **4** (456 mg, 1.14 mmol, 1 eq.), MeOH (15 mL), and  $K_2CO_3$  (631 mg, 4.56 mmol, 4 eq.) were added to a round bottom flask and stirred under Ar at rt for 2 h. At which time, the reaction was diluted with EtOAc (15 mL), filtered with cotton, and concentrated *in vacuo* to afford compound **5** as a tan powder (360 mg 87.5%). <sup>1</sup>H NMR (400 MHz, Chloroform-d):  $\delta$  6.95 (s, 1H), 6.68 (s, 1H), 3.81 (s, 4H), 3.80 (s, 4H), 3.31 (t,

1H), 2.83 (t, 1H), 1.42 – 1.37 (m, 10H). <sup>13</sup>**C NMR** (101 MHz, CDCl<sub>3</sub>): δ 155.87, 148.35, 148.18, 130.23, 115.55, 115.18, 114.44, 114.20, 113.45, 80.94, 79.19, 77.41, 77.29, 77.09, 76.77, 56.11, 55.99, 53.41, 36.02, 29.64, 28.38, 27.99, 27.84, 27.39, 22.15.

#### 4-(2-aminoethyl)-5-bromobenzene-1,2-diol

Compound **5** (360 mg, 0.999 mmol, 1 eq.) was dissolved in anhydrous  $CH_2Cl_2(10.5 \text{ mL})$  in a round bottom flask under Ar at rt and then cooled to -78°C. BBr<sub>3</sub> (1 M in  $CH_2Cl_2$ , 2.00 mL, 2.00 mmol, 2 eq.) was added dropwise. After 15 min, the reaction flask was allowed to warm to rt and the reaction continued for 2.5 h. At that time, the reaction was quenched with MeOH (1.5 mL) and stirred at rt for 1.5 h. The crude product was concentrated *in vacuo*, run through vacuum with diethyl ether and collected by filtration to afford **6** as a grey white powder (303 mg 96.8%). <sup>1</sup>**H NMR** (400 MHz,  $CD_3OD$ ):  $\delta$  6.97 (s, 1H), 6.77 (s, 1H), 3.10 (t, J = 7.9 Hz, 2H), 2.94 (t, J = 9.4, 6.4 Hz, 2H). <sup>13</sup>**C NMR** (101 MHz,  $CD_3OD$ ):  $\delta$  145.61, 145.29, 126.21, 118.97, 116.99, 116.97, 111.83, 48.22, 48.00, 47.79, 47.58, 47.36, 47.15, 46.94, 39.31, 32.84. The <sup>1</sup>H and <sup>13</sup>C NMR values matched those previously reported in the literature.<sup>31</sup>

### Determination of pKa for dopamine and 6-substituted derivatives

Each dopamine derivative was diluted from a DMSO stock and evaluated spectroscopically at a final concentration of 0.1-0.2 mM in argon-purged buffer solutions of constant ionic strength (0.1 M KCl) over a pH range of 2.98 to 10.01.<sup>47</sup> Acetate buffer was used from pH 3 to 5, phosphate buffer from pH 6 to 8, and borax buffer above pH 8. The UV-spectra were recorded at room temperature (30°C) on a Synergy HTX Multimode Microplate Reader between 210 nm and 600 nm at 2 nm resolution, using the 96-well microtiter plate method.<sup>47</sup> Raw UV data were imported into and processed with Microsoft Excel as follows: (1) UV-spectra of the analyte compounds were corrected by subtracting the UV-spectra of the blank solutions; (2) The raw scans were normalized (Abs<sub>600</sub> nm = 0); (3) The spectral difference between the acid spectrum (e.g., pH 2.0, 3.0 or 4.0) and the spectra at every other pH was plotted;

(4) The wavelengths of maximum positive and/or negative absorbance were determined graphically from the spectral difference plot; (5) The total absorbance difference at the chosen wavelengths was plotted against the pH. The data were fit with a derivation of the Henderson-Hasselbach equations as described by Tomsho and Benkovic<sup>48</sup> using Origin 6.0 (Microcal).

# Overexpression, purification, and reconstitution of *S. lincolnensis* L-DOPA 2,3-dioxygenase

Antibiotics, buffer components, and all reagents were from Sigma-Aldrich,
ThermoFisher, Lab Scientific or Bio-Rad. The basic molecular biology procedures for
bacterial growth, plasmid preparation and transformation of competent cells were
performed as described by Sambrook et al.<sup>49</sup>

Fifteen to twenty mL of LB medium ((Lab Scientific or Thermofisher) containing 200 µg/mL of ampicillin was inoculated with a single colony of transformed E. coli BL21 (DE3) cells (Thermofisher) containing pET16B1.50,51 The culture was incubated overnight at 37°C with agitation (220-225 rpm). On the next day, 1 L of LB media containing 200 µg/mL ampicillin was inoculated with 15-20 mL of the starter culture. The cells were grown with shaking at 37°C until the culture reached an  $A_{600}$  of ~0.6-0.8. The temperature was then reduced to 18°C, isopropyl-β-thiogalactoside was added to a final concentration of 0.1 mM and the culture was incubated for an additional 18 hours. The cells were then harvested by centrifugation at 5,000 x g for 20-30 min at 4°C and stored at -80°C. The frozen cells were thawed and resuspended at 5 mL per gram wet cells in phosphate buffer (50 mM, pH 8) containing sodium chloride (300 mM), imidazole (10 mM), glycerol (20%), and Triton-X100 (0.2%) at pH 8.0. The chilled suspension was disrupted on ice using sonication followed by disruption in a bead mill with 0.1 mm glass beads (BioSpec Products, Bartlesville, OK) according to the manufacturer's recommendations. The supernatant was clarified to remove cell debris and beads by centrifugation at 11,400 x g for 30 min at 4°C. The cell free crude extract containing

poly-histidine tagged L-DOPA dioxygenase was passed through 1.0 µm and 0.45 µm filters before purification by Ni-NTA affinity chromatography at RT by way of a Profinia purification system (BioRad) equipped with a 5 mL IMAC cartridge and operating under the native IMAC method with the following buffers for purification: Lysis/Wash 1 (50 mM KH<sub>2</sub>PO<sub>4</sub>, 300 mM KCl, 5 mM imidazole pH 8), Wash Buffer 2 (50 mM KH<sub>2</sub>PO<sub>4</sub>, 300 mM KCl, 10 mM imidazole pH 8) and Elution Buffer (50 mM KH<sub>2</sub>PO<sub>4</sub>, 300 mM KCl, 250 mM imidazole pH 8). Purified wild-type LmbB1 was frozen at -80°C in Elution buffer containing 10% glycerol. Purified wild-type L-DOPA dioxygenase were reconstituted with Fe<sup>II</sup> prior to enzymatic assay by incubating purified protein in the presence of 50 mM phosphate, 12.5 mM ascorbate, 300 mM NaCl, 250 mM imidazole, and FeSO<sub>4</sub>•7H<sub>2</sub>O in 3-5 molar excess of the protein at pH 8 for 10-30 min on ice. The reconstituting agents were removed by gel filtration with an Econo Pac 10DG column (BioRad) or a HiTrap Desalting cartridge (Cytiva), and the colorless protein was eluted into 50 mM HEPES buffer (pH 7.50) and glycerol (10%) ionic strength balanced to 0.154 M.

Wild-type purified, reconstituted *S. lincolnensis* L-DOPA dioxygenase could be aliquoted and stored at -80°C. L-DOPA dioxygenase protein was quantified using the Bradford assay (Coomassie Better Bradford<sup>TM</sup> assay (ThermoFisher) or by unfolding the protein in 6M Guanidine hydrochloride and determining concentration from  $A_{280}$  and an extinction of  $\epsilon_{M GdnHC} = 36,130 \ M^{-1} cm^{-1}$  for the unfolded protein. The Fe<sup>II</sup> content of purified or reconstituted L-DOPA dioxygenase was measured using a calibrated Ferrozine<sup>TM</sup> assay as previously described. All concentration measurements were made in triplicate, and errors were calculated as standard deviations.

# Mass Spectrometry of dopamine and 6-substituted derivatives and their reactions with L-DOPA dioxygenase

Evidence of L-DOPA dioxygenase cleavage was confirmed using electrospray-ionization mass spectrometry using an Advion Expression CMS operating with nitrogen flow. Purified L-DOPA dioxygenase was reconstituted, buffer exchanged

into 10 mM HPLC-grade ammonium bicarbonate buffer (pH ~8), and diluted to 200 μM. Analyte solutions were prepared at a concentration of 200 µM in the same buffer and adjusted to pH 6 (pH 8 for CHAPCA and cyanoCHAP) with HPLC-grade formic acid. Enzyme and substrate solutions were combined in equal parts and the reaction mixture incubated for 10 min, at which point enzyme was removed by ultrafiltration (0.5 mL Amicon ultrafiltration tube at 14,000 x g). The filtrate was stored at -80°C or used immediately. The MS was calibrated in positive and negative ion modes with capillary temperatures of 150-250°C. Solutions were injected (20 µL) via an isocratic pump into the mobile phase (50:50 solution of HPLC-grade methanol and Milli-Q water by volume) with a flow rate of 0.2 mL/min. Data were collected at a capillary temperature of 100 or 150°C in positive and negative ion modes. With the exception of 6-nitrodopamine and the reaction with L-DOPA dioxygenase which were detected in negative ion mode, all other spectra were collected in positive ion mode. Product spectra were analyzed using Advion Mass Express software by subtracting background signals from methanol, Milli-Q water, buffer and a substrate standard when analyzing reaction data. For hydroxydopamine, analyte spectra were obtained anaerobically as described above. In order to stabilize the rapidly oxidized hydroxydopamine structure, 1 mM sodium ascorbate was added to methanol, Milli-Q water, and buffer in accordance with previous studies,<sup>34</sup> but according to the MS data, it did not prevent oxidation.

# UV-visible spectroscopy and steady-state assay of L-DOPA dioxygenase

With the exception of 6-bromodopamine (see *Synthesis of 6-bromodopamine*), dopamine analogs were synthesized as previously described. Dopamine hydrochloride and 6-hydroxydopamine hydrobromide were purchased from Sigma-Aldrich. Michaelis-Menten steady-state constants  $K_M$ ,  $k_{cat}$ , and  $V_{max}$  were obtained by reacting L-DOPA dioxygenase (0.25-1  $\mu$ M) with dopamine analogs in reaction buffer (50 mM HEPES, 10% glycerol, pH 7.50), and by detecting the formation of the steady-state products at their respective  $\lambda_{max}$ . Medical-grade molecular oxygen (AirGas) was bubbled

directly into substrate solutions or reaction buffer through a glass-bonded silica gas diffuser (Bubblemac Industries, Inc.) or as a gas mixture blended with medical-grade air (Precision Medical). Solutions were bubbled for several min prior to use and for the duration of the experiment. Because dopamine and synthetic dopamine derivatives exhibited substrate and product inhibition in steady state assays, kinetic constants were extracted by global fitting of progress curves using Kintek Explorer (see *Data analysis and global modeling of the kinetic mechanism*).

To determine the  $K_M$  for oxygen, L-DOPA dioxygenase (0.25-1.0  $\mu$ M) was reacted with saturating dopamine/derivative (sufficient to achieve k<sub>cat</sub>) and various oxygen concentrations (21-100% or 270-1300 µM at 22°C). In the case of 6-carboxydopamine, the  $K_M$  of the compound was so high, that it was not possible to solubilize the substrate at concentrations that were in 10-fold excess of  $K_M$ . In this case, the  $K_{M,O2}$  was determined at the K<sub>M</sub> concentration for 6-carboxydopamine, and similar datasets were collected on dopamine and 6-bromodopamine for the purposes of comparison. The concentration of oxygen was varied by changing the percentage of oxygen in the blend using a galvanic oxygen sensor and oxygen monitor (Precision Medical) and then bubbling solutions as described above. Molecular oxygen percentages were converted to molar concentrations using a reference temperature of 22°C. The reaction of L-DOPA dioxygenase with dopamine/derivative as a function of oxygen concentration was followed by the appearance of the steady state cleavage product using UV-Visible spectroscopy. Initial rates were obtained from the slopes of the linear regions of the progress curves and plotted versus substrate concentration to yield a hyperbola, which was fit to the following alternative derivation of the Michaelis-Menten expression:  $\upsilon$  = (k<sub>cat</sub>[S])/(1+k<sub>SP</sub> [S]/k<sub>cat</sub>)<sup>37</sup> using standard nonlinear regression (Origin 6.0, Microcal) to obtain  $k_{SP}$  (or  $k_{cat}/K_M$ ) directly;  $K_M$  was calculated from the fitted  $k_{SP}$  and  $k_{cat}$  parameters according to the following expression:  $K_M = k_{cat}/k_{SP}$ .

Extinction coefficients for steady state cleavage products of dopamine and synthetic dopamine derivatives were determined by reacting various concentrations of the

dopamine/derivative at 22°C with a 10-fold stoichiometric excess of enzyme (quantified by Fe<sup>II</sup> - see *Overexpression*) in pH 7.5 50 mM HEPES buffer with 154 mM NaCl, bubbled with 100% molecular oxygen to a final concentration of 780-910 μM, depending on the volume of oxygenated buffer that comprised the reaction (60-70%). Substrate solutions were prepared from authentic, synthetic standards using an analytical balance.

### Anaerobic steady-state assay of L-DOPA dioxygenase

Catecholate formation was observed by reacting L-DOPA dioxygenase with dopamine analogs under anaerobic conditions. Reconstituted L-DOPA dioxygenase was gel filtered into reaction buffer (50 mM HEPES pH 7.5) degassed on a vacuum pump and diluted to 100 µM. Substrate stock solution was prepared in the same buffer, and both stock solutions were covered with rubber septa and purged with argon to displace oxygen in solution. The substrate was bubbled directly, and the headspace of the enzyme solution was aerated to displace oxygen without destabilizing the protein.  $\alpha$ -D-Glucose (0.069 M) (Fisher Scientific) and a 50  $\mu$ M oxygen scavenger cocktail composed of glucose oxidase (Sigma-Aldrich) and catalase (Sigma-Aldrich) was added to both the enzyme and substrate, and solutions were again purged with argon. An aliquot of substrate was transferred to a cuvette containing degassed reaction buffer and covered with a rubber septum, and allowed to further deoxygenate. A 1 mL syringe attached to a needle was then used to transfer 800 µL of L-DOPA dioxygenase jacketed between 100 µL of argon gas on either side, dispensed through cuvette septa. Reaction volume was kept constant at 1 mL, and reactions were monitored over a wavelength range of 280-600 nm. A substrate-only blank was subtracted from all experimental traces to eliminate substrate interference. The change in absorbance was visualized over time in a UV-1800 (Shimadzu).

#### Pre-steady state assay of L-DOPA dioxygenase with dopamine

Pre-steady state observation of the L-DOPA dioxygenase reaction with dopamine was carried out on a SF300x stopped-flow spectrometer (KinTek Corporation). Reaction temperature was controlled at either  $12 \pm 1^{\circ}$ C or  $20 \pm 1^{\circ}$ C by a circulating water bath. HEPES buffers (50 mM) for these reactions were balanced for ionic strength with NaCl and titrated with HCl or NaOH such that the pH would be 7.5 at the reaction temperature. The instrument drive syringes were cleaned with acid, base, and water, and flushed with reaction buffer before each use. The same buffer was used to reference the instrument at the desired wavelength of observation. Stock solutions of dopamine (5.0 mM) were prepared in acidified Milli-Q water (pH 3) to prevent oxidation. The reaction buffer was bubbled with 100% O<sub>2</sub> in the temperature-controlled bath for at least 10 minutes, and dopamine solutions were prepared by diluting the stock into the oxygenated buffer to the desired concentration immediately prior to loading on the instrument (syringe C). L-DOPA dioxygenase reconstituted with iron (II) sulfate heptahydrate and gel filtered into the reaction buffer was prepared and diluted, if necessary, and loaded into drive syringe A. For each reaction, the instrument mixes 20 µL of each reactant (1:1 dilution), which was observed at either 360 nm to detect the formation of AEHMS. Fifteen to twenty progress curves from the same experimental conditions were averaged in the KinTek Stopped Flow software and exported to KinTek Explorer for modeling.

#### Data analysis and global modeling of the kinetic mechanism

Kinetic data were analyzed by fitting to simulated mechanisms using the KinTek Explorer software (KinTek Corp, Austin, TX). <sup>52</sup> KinTek Explorer simulates experimental results by using direct numerical integration of rate equations for the kinetic model and yields estimates for the rate constants of microscopic steps.

For the purpose of extracting  $k_{cat}$  and  $K_{M}$ , progress curve experiments from steady-state kinetics assays were globally fit to model (i) using KinTek Explorer,<sup>37,52</sup> where E =

L-DOPA dioxygenase, S = dopamine derivative, and P = enzymatic product. The model does not solve for individual rates, rather it gives a macroscopic view of the effects of inhibition on  $K_M$  ( $k_1/100$ ) and  $k_{cat}$  ( $k_2$ ). Within each experiment, the data for a single condition were normalized and averaged. Standard deviations for each condition were manually calculated and imported into KinTek Explorer. Each steady-state dataset included a 2.0 second dead time consistent with manual data collection. Extinction coefficients were independently determined (Table 3) and fixed during fitting of steady-state datasets. Vertical scaling factors were used and fixed during fitting. Reverse rates k<sub>-2</sub> and k<sub>-3</sub> were fixed to zero to limit the variables in the model and ensure the data were sufficient to constrain the rates. k<sub>3</sub> was fixed to be very fast and k<sub>1</sub> was fixed to 100 so the estimate of  $K_M$  is equivalent to  $k_{-1}/100$ . Simple substrate  $(k_4, k_{-4})$ inhibition was added and the equilibrium ratio of k<sub>4</sub>/k<sub>4</sub> was fixed at 1. Simple product inhibition was modeled with k<sub>5</sub> (k<sub>.5</sub> was fixed at zero to limit the variables in the model and ensure the data were sufficient to constrain the rates). Errors were calculated from 2D Fitspace<sup>53</sup> at 0.83 Chi<sup>2</sup>, with all scaling factors locked. The KinTek Explorer program FitSpace explores the uniqueness of a particular fit to the data by measuring the dependence of the sum square error (SSE) on each pair of parameters, while allowing all other parameters to vary in seeking the best fit 53 The confidence intervals reported for each of the fitted parameters are determined by a Chi<sup>2</sup> Threshold of 0.83 (SSE<sub>x,y</sub> / SSE<sub>min</sub>) and include the range of values for which the fits have X<sup>2</sup> that deviate values no more than 20% from the lowest X<sup>2</sup> value. These confidence intervals are also represented as two-dimensional plots (confidence contours) of the reciprocal sum square error (SSE<sub>min</sub> / SSE<sub>x,v</sub>); constrained parameters have a well-defined region in which the SSE<sub>x,y</sub> approaches SSE<sub>min</sub> (red color in a contour plot).

$$E + S \xrightarrow{k_{1} (100)} ES \xrightarrow{k_{2} (0)} EP \xrightarrow{k_{3} (fast)} E + P$$

$$S \qquad P \qquad (i)$$

$$k_{5} \downarrow k_{-5} (0) \qquad k_{4} \downarrow k_{-4} (K_{4} = 1)$$

$$SES \qquad PEP$$

Pre-steady state experiments were modeled using Kintek Explorer to a reaction pathway based on Figure 2 and shown below in model (ii). Fits were evaluated by Fitspace confidence contour analysis.

$$E1 + S \xrightarrow{k_{2}} ES1 \xrightarrow{k_{3} (fast)} ESO_{2} \xrightarrow{k_{4} (fast)} ESQ \xrightarrow{k_{6}} ESQ_{2}X$$

$$k_{1} \downarrow k_{1} \downarrow$$

# **Associated Content:**

#### Supporting Information

The supporting information contains Figures S1-S11 and supplemental methods. Figure S1 shows the structures of all dopamine derivatives, Figure S2 illustrates the results of the docking experiments with 6ON3. Figure S3 contains data and fits used to extract pKas, and Figures S4 & S5 shows the MS data of substrates and products for all enzymatic reactions described herein. Figures S7 through S9 are data and fits for steady state kinetics and extinction coefficients. Figures S8 and S9 illustrate specific oxygen dependent and anaerobic experiments on dopamine derivatives. Figure S12 includes enlarged versions of the FitSpace confidence contour analyses presented in Figure 4.

#### **Accession Codes**

S. lincolinensis L-DOPA dioxygenase CAA55747.1

# Acknowledgements

The authors acknowledge William Eckenhoff (Rhodes College) for assistance with cyclic voltammetry experiments.

# References

- (1) Bugg, T. D., Ahmad, M., Hardiman, E. M., and Singh, R. (2011) The emerging role for bacteria in lignin degradation and bio-product formation. *Curr. Opin. Biotechnol.* 22, 394–400. (2) Kamimura, N., Takahashi, K., Mori, K., Araki, T., Fujita, M., Higuchi, Y., and Masai, E. (2017) Bacterial catabolism of lignin-derived aromatics: New findings in a recent decade: Update on bacterial lignin catabolism. *Environ. Microbiol. Rep.* 9, 679–705.
- (3) Wu, W., Dutta, T., Varman, A. M., Eudes, A., Manalansan, B., Loqué, D., and Singh, S. (2017) Lignin Valorization: Two Hybrid Biochemical Routes for the Conversion of Polymeric Lignin into Value-added Chemicals. *Sci. Rep.* 7, 8420.
- (4) He, P., and Moran, G. R. (2011) Structural and mechanistic comparisons of the metal-binding members of the vicinal oxygen chelate (VOC) superfamily. *J. Inorg. Biochem.* 105, 1259–1272.
- (5) Barry, K. P., and Taylor, E. A. (2013) Characterizing the Promiscuity of LigAB, a Lignin Catabolite Degrading Extradiol Dioxygenase from Sphingomonas paucimobilis SYK-6. *Biochemistry 5*2, 6724–6736.
- (6) Fetzner, S. (2012) Ring-Cleaving Dioxygenases with a Cupin Fold. *Appl. Environ. Microbiol.* 78, 2505–2514.
- (7) Burroughs, A. M., Glasner, M. E., Barry, K. P., Taylor, E. A., and Aravind, L. (2019) Oxidative opening of the aromatic ring: tracing the natural history of a large superfamily of dioxygenase domains and their relatives. *J. Biol. Chem.* jbc.RA119.007595.
- (8) Wolgel, S. A., Dege, J. E., Perkins-Olson, P. E., Jaurez-Garcia, C. H., Crawford, R. L., Munck, E., and Lipscomb, J. D. (1993) Purification and characterization of protocatechuate 2,3-dioxygenase from Bacillus macerans: a new extradiol catecholic dioxygenase. *J Bacteriol* 175, 4414–26.
- (9) Colabroy, K. L., Horwitz, A. D., Basciano, V. R., Fu, Y., Travitz, K. M., Robinson, M. K., Shimanski, B. A., and Hoffmann, T. W. (2019) A New Way of Belonging: Active-Site Investigation of L-DOPA Dioxygenase, a VOC Family Enzyme from Lincomycin Biosynthesis. *Biochemistry 58*, 4794–4798.
- (10) Miller, M. A., and Lipscomb, J. D. (1996) Homoprotocatechuate 2,3-dioxygenase from Brevibacterium fuscum. A dioxygenase with catalase activity. *J Biol Chem 271*, 5524–35.
- (11) Eltis, L. D., Hofmann, B., Hecht, H. J., Lunsdorf, H., and Timmis, K. N. (1993) Purification and crystallization of 2,3-dihydroxybiphenyl 1,2-dioxygenase. *J Biol Chem* 268, 2727–32.
- (12) Ishida, T., Tanaka, H., and Horiike, K. (2004) Quantitative Structure-Activity Relationship for

- the Cleavage of C3/C4-Substituted Catechols by a Prototypal Extradiol Catechol Dioxygenase with Broad Substrate Specificity. *J. Biochem. (Tokyo)* 135, 721–730.
- (13) McKay, D. B., Prucha, M., Reineke, W., Timmis, K. N., and Pieper, D. H. (2003) Substrate Specificity and Expression of Three 2,3-Dihydroxybiphenyl 1,2-Dioxygenases from Rhodococcus globerulus Strain P6. *J. Bacteriol.* 185, 2944–2951.
- (14) Kovaleva, E. G., Rogers, M. S., and Lipscomb, J. D. (2015) Structural Basis for Substrate and Oxygen Activation in Homoprotocatechuate 2,3-Dioxygenase: Roles of Conserved Active Site Histidine 200. *Biochemistry 54*, 5329–5339.
- (15) Vaillancourt, F. H., Fortin, P. D., Labbé, G., Drouin, N. M., Karim, Z., Agar, N. Y. R., and Eltis, L. D. (2005) Molecular basis for the substrate selectivity of bicyclic and monocyclic extradiol dioxygenases. *Biochem. Biophys. Res. Commun.* 338, 215–222.
- (16) Sutherlin, K. D., Wasada-Tsutsui, Y., Mbughuni, M. M., Rogers, M. S., Park, K., Liu, L. V., Kwak, Y., Srnec, M., Böttger, L. H., Frenette, M., Yoda, Y., Kobayashi, Y., Kurokuzu, M., Saito, M., Seto, M., Hu, M., Zhao, J., Alp, E. E., Lipscomb, J. D., and Solomon, E. I. (2018) NRVS definition of O2 intermediates in an extradiol dioxygenase: correlation to crystallography and reactivity. *J. Am. Chem. Soc. 140*, 16495–16513.
- (17) Kovaleva, E. G., and Lipscomb, J. D. (2007) Crystal structures of Fe2+ dioxygenase superoxo, alkylperoxo, and bound product intermediates. *Science 316*, 453–457.
- (18) Mbughuni, M. M., Chakrabarti, M., Hayden, J. A., Bominaar, E. L., Hendrich, M. P., Münck, E., and Lipscomb, J. D. (2010) Trapping and spectroscopic characterization of an Felll-superoxo intermediate from a nonheme mononuclear iron-containing enzyme. *Proc. Natl. Acad. Sci.* 107, 16788–16793.
- (19) Mbughuni, M. M., Chakrabarti, M., Hayden, J. A., Meier, K. K., Dalluge, J. J., Hendrich, M. P., Münck, E., and Lipscomb, J. D. (2011) Oxy Intermediates of Homoprotocatechuate 2,3-Dioxygenase: Facile Electron Transfer between Substrates. *Biochemistry 50*, 10262–10274. (20) Mbughuni, M. M., Meier, K. K., Munck, E., and Lipscomb, J. D. (2012) Substrate-mediated oxygen activation by homoprotocatechuate 2,3-dioxygenase: intermediates formed by a tyrosine 257 variant. *Biochemistry 51*, 8743–54.
- (21) Vaillancourt, F. H., Barbosa, C. J., Spiro, T. G., Bolin, J. T., Blades, M. W., Turner, R. F., and Eltis, L. D. (2002) Definitive evidence for monoanionic binding of 2,3-dihydroxybiphenyl to 2,3-dihydroxybiphenyl 1,2-dioxygenase from UV resonance Raman spectroscopy, UV/Vis absorption spectroscopy, and crystallography. *J Am Chem Soc* 124, 2485–96.
- (22) Vaillancourt, F. H., Labbé, G., Drouin, N. M., Fortin, P. D., and Eltis, L. D. (2002) The Mechanism-based Inactivation of 2,3-Dihydroxybiphenyl 1,2-Dioxygenase by Catecholic Substrates. *J. Biol. Chem.* 277, 2019–2027.
- (23) Shu, L., Chiou, Y.-M., Orville, A. M., Miller, M. A., Lipscomb, J. D., and Que Jr, L. (1995) X-ray absorption spectroscopic studies of the Fe (II) active site of catechol 2, 3-dioxygenase. Implications for the extradiol cleavage mechanism. *Biochemistry 34*, 6649–6659.
- (24) Viggiani, A., Siani, L., Notomista, E., Birolo, L., Pucci, P., and Di Donato, A. (2004) The Role of the Conserved Residues His-246, His-199, and Tyr-255 in the Catalysis of Catechol 2,3-Dioxygenase from Pseudomonas stutzeri OX1. *J. Biol. Chem.* 279, 48630–48639.
- (25) Colabroy, K. L. (2016) Tearing down to build up: Metalloenzymes in the biosynthesis lincomycin, hormaomycin and the pyrrolo [1,4]benzodiazepines. *Biochim. Biophys. Acta BBA Proteins Proteomics* 1864, 724–737.
- (26) Wang, Y., Shin, I., Fu, Y., Colabroy, K. L., and Liu, A. (2019) Crystal Structures of L-DOPA Dioxygenase from Streptomyces sclerotialus. *Biochemistry* 58, 5339–5350.
- (27) Dannhardt, G., and Kiefer, W. (2001) 1-Pyrrolines (3,4-dihydro-2H-pyrroles) as a template for new drugs. *Arch. Pharm. (Weinheim)* 334, 183–188.

- (28) S. Medran, N., La-Venia, A., and A. Testero, S. (2019) Metal-mediated synthesis of pyrrolines. *RSC Adv.* 9, 6804–6844.
- (29) Ulanova, D., Novotná, J., Smutná, Y., Kameník, Z., Gažák, R., Šulc, M., Sedmera, P., Kadlčík, S., Plháčková, K., and Janata, J. (2010) Mutasynthesis of Lincomycin Derivatives with Activity against Drug-Resistant Staphylococci. *Antimicrob. Agents Chemother. 54*, 927–930.
- (30) Yonemoto, I. T., Li, W., Khullar, A., Reixach, N., and Gerratana, B. (2012) Mutasynthesis of a potent anticancer sibiromycin analogue. *ACS Chem Biol* 7, 973–7.
- (31) Rote, J. C., Malkowski, S. N., Cochrane, C. S., Bailey, G. E., Brown, N. S., Cafiero, M., and Peterson, L. W. (2017) Catechol reactivity: Synthesis of dopamine derivatives substituted at the 6-position. *Synth. Commun.* 47, 435–441.
- (32) Lipscomb, J. D. (2008) Mechanism of extradiol aromatic ring-cleaving dioxygenases. *Curr. Opin. Struct. Biol.* 18, 644–649.
- (33) Wang, Y., Liu, K. F., Yang, Y., Davis, I., and Liu, A. (2020) Observing 3-hydroxyanthranilate-3,4-dioxygenase in action through a crystalline lens. *Proc. Natl. Acad. Sci. 117*, 19720–19730.
- (34) Mastro, K. J., Zitelli, K. T., Willard, A. M., Leblanc, K. H., Kravitz, A. V., and Gittis, A. H. (2017) Cell-specific pallidal intervention induces long-lasting motor recovery in dopamine-depleted mice. *Nat. Neurosci.* 20, 815–823.
- (35) Schusler-Van Hees, M. T., Beijersbergen Van Henegouwen, G. M., and Driever, M. F.
- (1983) Ionization constants of catechols and catecholamines. *Pharm Weekbl Sci* 5, 102–8.
- (36) Wang, J., Wang, W., Kollman, P. A., and Case, D. A. (2006) Automatic atom type and bond type perception in molecular mechanical calculations. *J. Mol. Graph. Model.* 25, 247–260.
- (37) Johnson, K. A. (2019) New standards for collecting and fitting steady state kinetic data. *Beilstein J. Org. Chem.* 15, 16–29.
- (38) Barreto, W. J., Barreto, S. R. G., Ponzoni, S., Kawano, Y., Di Mauro, E., Magosso, H. A., and Silva, W. P. (2005) Preparation and Characterization of a Stable Semiquinone-Iron Complex. *Monatshefte Für Chem. Chem. Mon.* 136, 701–712.
- (39) Barreto, W. J., Silva, W. P., Scarmínio, I. S., Barreto, S. R. G., and Silva, L. F. S. (2007) A Spectroscopic and Kinetic Investigation on the Substitution of Fe(III) for Ni(II) in a Siderophore Model. *Z. Für Naturforschung B* 62, 685–690.
- (40) Colabroy, K. L., Smith, I. R., Vlahos, A. H. S., Markham, A. J., and Jakubik, M. E. (2014) Defining a kinetic mechanism for I-DOPA 2,3 dioxygenase, a single-domain type I extradiol dioxygenase from Streptomyces lincolnensis. *Biochim. Biophys. Acta BBA Proteins Proteomics* 1844, 607–614.
- (41) Arciero, D. M., Orville, A. M., and Lipscomb, J. D. (1985) [170]Water and nitric oxide binding by protocatechuate 4,5-dioxygenase and catechol 2,3-dioxygenase. Evidence for binding of exogenous ligands to the active site Fe2+ of extradiol dioxygenases. *J. Biol. Chem.* 260, 14035–14044.
- (42) Kiser, P. D. (2017) Reappraisal of dioxygen binding in NOV1 crystal structures. *Proc. Natl. Acad. Sci. 114*, E6027–E6028.
- (43) C. C. Huang, G. S. C. (1996) Chimera: An extensible molecular modeling application constructed using standard components.
- (44) Trott, O., and Olson, A. J. (2010) AutoDock Vina: Improving the speed and accuracy of docking with a new scoring function, efficient optimization, and multithreading. *J. Comput. Chem.* 31, 455–461.
- (45) Ribeiro, J. A., Fernandes, P. M. V., Pereira, C. M., and Silva, F. (2016) Electrochemical sensors and biosensors for determination of catecholamine neurotransmitters: A review. *Talanta 160*, 653–679.

- (46) Alarcón-Angeles, G., Corona-Avendaño, S., Palomar-Pardavé, M., Rojas-Hernández, A., Romero-Romo, M., and Ramírez-Silva, M. T. (2008) Selective electrochemical determination of dopamine in the presence of ascorbic acid using sodium dodecyl sulfate micelles as masking agent. *Electrochimica Acta* 53, 3013–3020.
- (47) Martínez, C. H. R., and Dardonville, C. (2012) Rapid Determination of Ionization Constants (pKa) by UV Spectroscopy Using 96-Well Microtiter Plates. *ACS Med. Chem. Lett. 4*, 142–145. (48) Tomsho, J. W., Pal, A., Hall, D. G., and Benkovic, S. J. (2012) Ring Structure and Aromatic Substituent Effects on the pKa of the Benzoxaborole Pharmacophore. *ACS Med. Chem. Lett. 3*, 48–52
- (49) Sambrook, J., Fritsch, E. F., and Maniatis, T. (1989) Molecular Cloning, A Laboratory Manual. Cold Spring Harbor Laboratory Press.
- (50) Neusser, D., Schmidt, H., Spizek, J., Novotna, J., Peschke, U., Kaschabeck, S., Tichy, P., and Piepersberg, W. (1998) The genes ImbB1 and ImbB2 of Streptomyces lincolnensis encode enzymes involved in the conversion of L-tyrosine to propylproline during the biosynthesis of the antibiotic lincomycin A. *Arch. Microbiol.* 169, 322–332.
- (51) Colabroy, K. L., Hackett, W. T., Markham, A. J., Rosenberg, J., Cohen, D. E., and Jacobson, A. (2008) Biochemical characterization of L-DOPA 2,3-dioxygenase, a single-domain type I extradiol dioxygenase from lincomycin biosynthesis. *Arch Biochem Biophys* 479, 131–8. (52) Johnson, K. A. (2009) Fitting enzyme kinetic data with KinTek Global Kinetic Explorer. *Methods Enzym.* 467, 601–26.
- (53) Johnson, K. A., Simpson, Z. B., and Blom, T. (2009) FitSpace explorer: an algorithm to evaluate multidimensional parameter space in fitting kinetic data. *Anal Biochem 387*, 30-41. (54) Kovaleva, E. G., and Lipscomb, J. D. (2012) Structural Basis for the Role of Tyrosine 257 of Homoprotocatechuate 2,3-Dioxygenase in Substrate and Oxygen Activation. *Biochemistry 51*, 8755–8763.

## **Figures**

Figure 1.

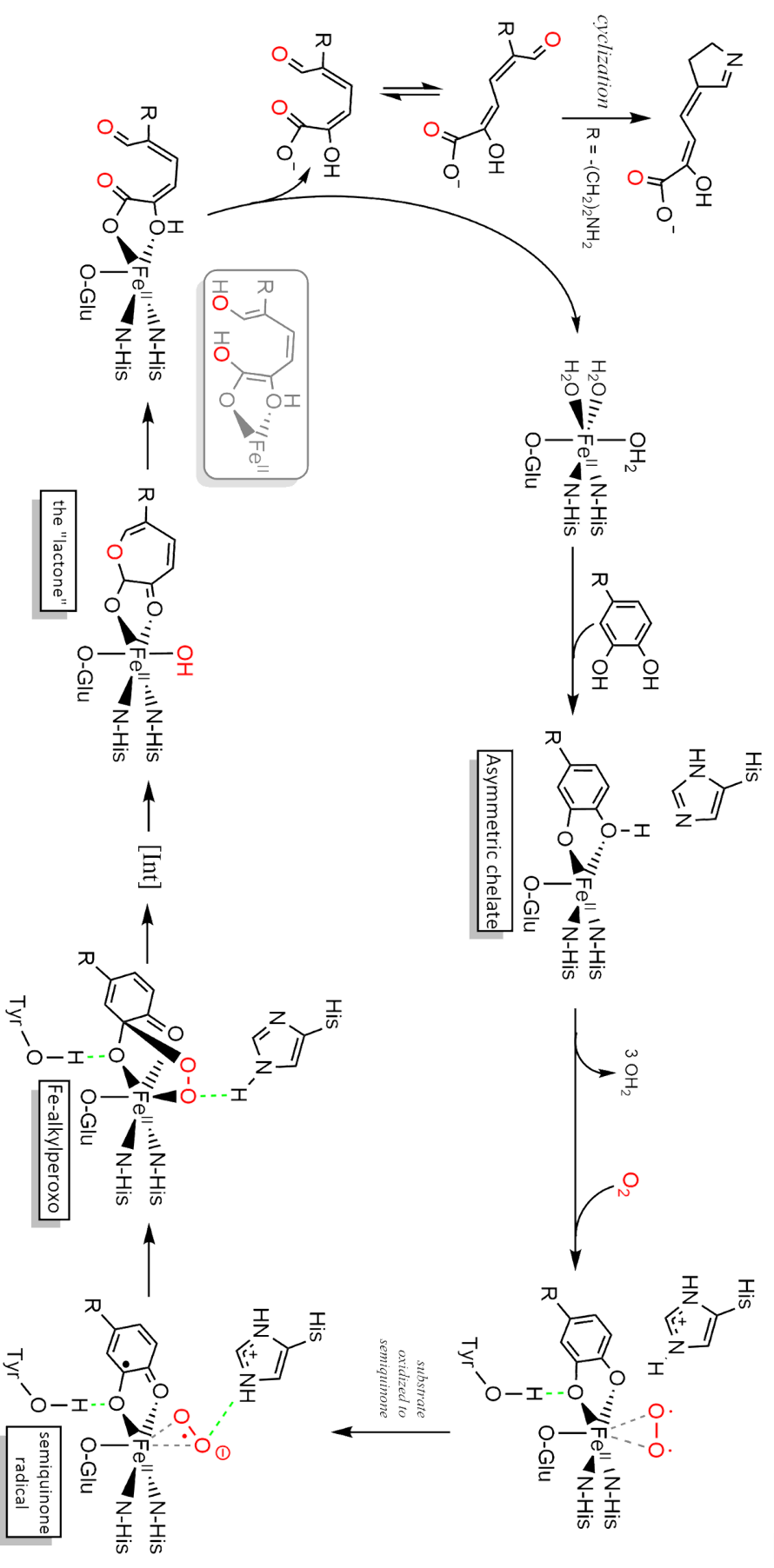


Figure 2.

Figure 3.

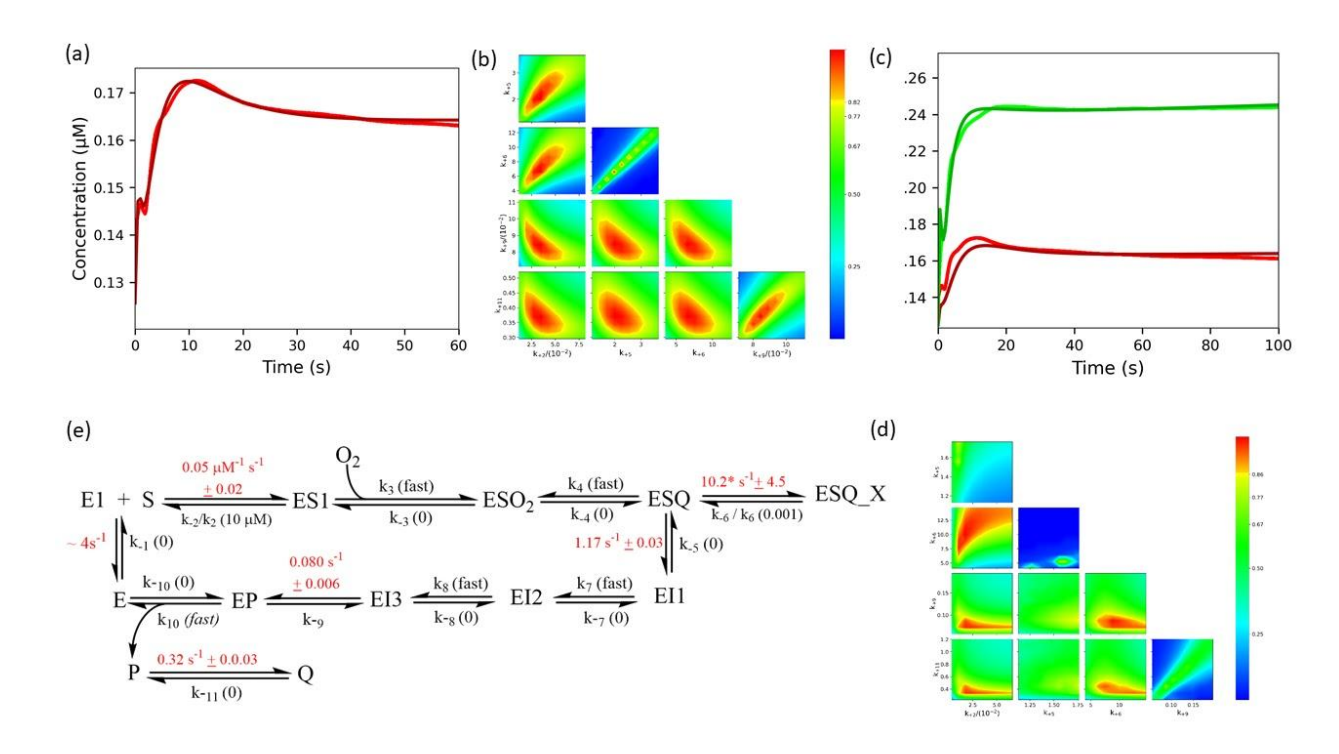


Figure 4.

## **Tables**

Table 1.

Compound	(E♭)ª (mV) Oxidation	(E♭)∘ (mV) Reduction	Oxidation/Reduction Mechanism	E1/2 (mV)
Dopamine (DA)	143	88	Reversible	115.5
6-hydroxyDA	-36	-375	Reversible	-205.5
6-bromoDA	175	137	Reversible	156
6-carboxyDA	241	81	Reversible	161
CyclicDA	242	79	Reversible	160.5
6-cyanoDA	285	233	Reversible	259
6-nitroDA	U.S.	319	Irreversible	-

Table 2.

Compound	pK <sub>a</sub> 1 (C3-O-H)	pK <sub>a</sub> 2 (C4-O-H)	pK <sub>a</sub> N (H-NHR <sub>2</sub> )
Dopamine	8.99 ± 0.13	> 10	
6-carboxyDA	$8.14 \pm 0.08$	> 10	
CyclicDA	8.27 ± 0.18	> 10	5.79 ± 0.12
6-bromoDA	8.15 ± 0.11	> 10	
6-cyanoDA	7.23 ± 0.09	> 9	
6-nitroDA	6.32 ± 0.03	> 9	

Table 3.

Compound	K <sub>M DOPA/DA/6-x-DA</sub> (μM )	k <sub>cat</sub> (sec <sup>-1</sup> )	K <sub>M</sub> O <sub>2</sub> (μM )	k <sub>sp</sub> O <sub>2</sub> (μM <sup>-1</sup> min <sup>-1</sup> ) <sup>h</sup>	λ <sub>max</sub> of steady state product	Extinction Coefficient at $\lambda_{max}$ (M <sup>-1</sup> cm <sup>-1</sup> )
L-DOPA	27.3 ± 2.1 <sup>f</sup> 35.8 ± 1.8 <sup>g</sup>	1.03 ± 0.12 <sup>f</sup> 1.27 ± 0.11 <sup>g</sup>	53.2 ± 1.6 <sup>e</sup> 3.1 ± 7.4 <sup>d</sup>	0.84 ± 0.02° 27.2 ± 64.7 <sup>d</sup>	414 nm	47,500° 44,560 <sup>b</sup>
Dopamine	120 ± 27 <sup>f</sup> 571 ± 144 <sup>g</sup>	8.7 ± 1.6 <sup>f</sup> 1.49 ± 0.3 <sup>g</sup>	982 ± 198° 499 ± 31 <sup>d</sup>	$0.051 \pm 0.007^{\circ}$ $0.20 \pm 0.01^{d}$	433 nm	29,690 ± 520
6-bromoDA	118 ± 31 <sup>f</sup> 	1.32 ± 0.25 <sup>f</sup>	296 ± 35° 48.2 ± 17.2 <sup>d</sup>	0.18 ± 0.02 <sup>c</sup> 2.5 ± 0.9 <sup>d</sup>	429 nm	27,030 ± 360
6-carboxyDA	3640 ± 1510 <sup>f</sup>	0.77 ± 0.20 <sup>f</sup>	240 ± 11°	0.071 ±0.003°	425 nm	30,150 ± 940
cyclicDA	n.d.	n.d.	n.d.	n.d.	429 nm	n.d.
6-cyanoDA	264 ± 44 <sup>f</sup> 438 ± 49 <sup>g</sup>	$1.00 \pm 0.06^{f}$ $0.59 \pm 0.03^{g}$	845 ± 114 <sup>d</sup>	0.135 ± 0.012 <sup>d</sup>	435 nm	23,840 ± 160
6-nitroDA	n.d.	n.d.	n.d.	n.d.	365 nm	n.d.

Table 4.

Reaction pathway	Dopamine 100 % ${\rm O_2}$ 21% ${\rm O_2}$	6-cyanodopamine $100~\%~\mathrm{O_2}$ $21\%~\mathrm{O_2}$	6-bromodopamine 100 % O <sub>2</sub>	6-carboxydopamine 100 % O <sub>2</sub>
E + S = ES (k <sub>-1</sub> /100)	120 ± 27 571 ± 144	264 ± 44 438 ± 49	118 ± 31	3640 ± 1510
$ES = EP (k_2 = k_{cat})$	8.7 ± 1.6 1.49 ± 0.3	$1.00 \pm 0.06$ $0.59 \pm 0.03$	1.32 ± 0.25	0.773 ± 0.20
$EP = E + P (k_3, product release)$	> 1E06 (fast)	> 1E06 (fast)	> 1E06 (fast)	> 1E06 (fast)
$E + P = PE (k_{-4} \& k_4)$	$0.0143 \pm 0.0016$ $0.0049 \pm 0.0012$	2.11E-03 ± 5.25E-04 2.74E-03 ± 3.90 E-04	0.0094 ± 0.0019	0.014 ± 0.005
$ES + S = SES (k_5)$	4.76E-05 ± 1.05E-05 3.21E-04 ± 7.0 E-05	1.35E-05 ± 2.6E-06 1.11E-05 ± 1.53E-06	6.4e-04 ± 1.7E-04	7.54E-06 ± 2.46E-06

<sup>&</sup>lt;sup>a</sup>Neusser, D. et al. Archives of microbiology **169**, 322–332 (1998). <sup>b</sup>Colabroy, K. L., Smith, I. R., Vlahos, A. H. S., Markham, A. J. & Jakubik, M. E. *Biochimica et Biophysica Acta (BBA) - Proteins and Proteomics* **1844**, 607–614 (2014).

 $<sup>^{\</sup>rm c}$  These constants were determined at dopamine concentrations that were at K<sub>M,DA/6-X-DA</sub>.

 $<sup>^{\</sup>rm d}$  determined in excess of the  $\rm K_M$  for L-DOPA (10x), DA (10x) or 6-X-DA (5-10x)

 $<sup>^</sup>e$  determined at 100  $\mu M$  or 3x the  $K_M$  for L-DOPA  $^f$  determined with 100%  $O_2$  saturation  $^g$  determined with air/21%  $O_2$  saturation

 $<sup>^{</sup>h}$ K<sub>SP</sub>is also k<sub>cat</sub>/K<sub>M</sub>(Johnson, 2019) n.d. – *not determined* 

## Figure Captions and Table Headings

**Figure 1.** Possible pathways and applications for EDX reaction with catecholic substrates.

Figure 2. A proposed mechanism for EDX cleavage of a catecholic substrate.<sup>20,32,33,54</sup> The substrate catechol is proposed to bind as a monoanion, displacing two molecules from around the Fe<sup>II</sup> to form the asymmetric chelate. The monoanionic nature of the substrate is a function of catecholic pKa. Alternative substrates with low catecholic pKa can bind as a dianion. The oxygen molecule binds to the Fe<sup>II</sup> displacing the final water molecule. Subsequently, the substrate is oxidized to the semiquinone radical via the metal ion. The radical iron-bound superoxo species and the semiquinone radical recombine to yield the Fe-alkylperoxo intermediate. O-O and C-C bond cleavage affords a ring expansion which likely proceeds in a stepwise manner through several additional intermediates (not shown). <sup>17,33</sup> The resulting lactone is hydrolyzed by the metal bound hydroxide to afford the ring-opened product. Tautomerization to the enol form is possible, <sup>33</sup> and the ring-opened product likely isomerizes upon release from the enzyme. If the R group contains an amino functionality, cyclization to an imine follows.

**Figure 3**. The L-DOPA dioxygenase catalyzed conversion of dopamine and 6-X-dopamines to 5-(3-aminoethyl)-2-hydroxy muconic semialdehyde (AEHMS), which cyclizes non-enzymatically to 3-(3-carboxy-3-hydroxy-allylidene)-4,5-dihydro-2H-pyrrole or CHAP. CHAP can isomerize and tautomerize.

Figure 4. Pre-steady state analysis of the dopamine reaction with L-DOPA dioxygenase. (a) Dopamine (30 μM) and L-DOPA dioxygenase (70 μM) at pH 7.5, 12°C, ~1000 µM O<sub>2</sub> and 360 nm produce a spectroscopic feature in the first second consistent with the transient accumulation of a semiguinone species with extinction of  $3,075 \pm 695$ M<sup>-1</sup> cm<sup>-1</sup>. The trace is fit to the model shown in (d) (b) 2D Fitspace confidence contour analysis for (a) based on the model in (d). (c) Dopamine (30 µM, 300 µM) and L-DOPA dioxygenase (70 μM) at pH 7.5, 12°C, ~1000 μM O<sub>2</sub> and 360 nm. The concentration dependence of the rates is consistent with the formation of a non-productive step along the reaction pathway, shown as k<sub>6</sub> in part (d). (e) FitSpace confidence contour analysis<sup>53</sup> for (c). (d) A reaction pathway consistent with Figure 2 and the data presented herein. The model includes a non-productive step after oxygen binding and along the reaction pathway shown as k<sub>6</sub>, which effectively reduces the amplitudes of the traces in part (c). Rates were fixed as either "fast" or zero as shown,  $k_2/k_2$  was fixed at 10,  $k_6/k_6$  was fixed at 0.001 and k₁ was fixed as ~4. Extinction coefficients were fitted and/or fixed during fitting as described in the text. The values shown in (d) come from the fit of the trace in part (a), with the exception of k<sub>6</sub> which came from the fit in part (c). E, E1 and S are the enzyme and substrate – binding prior to O<sub>2</sub>. ESO<sub>2</sub> is the ternary complex of enzyme, dopamine substrate and oxygen. ESQ represents the putative semiquinone intermediate, ESQ\_X is the non-productive intermediate discussed in the text, El1 through EI3 represent the Fe-alkylperoxo, additional putative intermediates, and the lactone shown in Figure 2. EP + P are the semialdehyde product in complex with the enzyme and after product release, and Q is the product of spontaneous cyclization of P to the pyrroline/dihydropyrrole (see Figure 3).

**Table 1.** Anodic (oxidation,  $(E_p)_a$ ) and cathodic (reduction,  $(E_p)_c$ ) peak potentials from cyclic voltammograms of dopamine or dopamine derivative solutions at in phosphate buffer, pH 7.4 on a GCE (d = 2 mm).

**Table 2.** Dopamine and synthetic dopamine derivatives were evaluated spectroscopically from pH 3 – 10 to determine pKa for one or both of the catecholic protons as described in the Materials and Methods. The wavelength of maximum absorbance change was plotted as a function of pH and fit with a derivation of the Henderson-Hasselbach equation as described.<sup>48</sup> Decomposition of the compounds prohibited data collection above pH 10.

**Table 3.** A summary of steady-state kinetic parameters,  $\lambda_{max}$  and extinction coefficients for the cleavage products of dopamine and 6-X-dopamine derivatives with respect to the native substrate L-DOPA. All steady state experiments were conducted at pH 7.5, 22°C and with 100% or 21%  $O_2$  saturation as indicated.

**Table 4.** Fits of steady state kinetic data to a simple "steady state" model<sup>37</sup> that includes simple substrate ( $k_{-4}$  &  $k_{-4}$ ) and simple product ( $k_{-5}$ ) inhibition as defined in the Materials and Methods. The model does not solve for individual rates, rather it gives a macroscopic view of the effects of inhibition on  $K_M$  ( $k_1/100$ ) and  $k_{cat}$  ( $k_2$ ).<sup>37</sup> Each dataset included a 2.0 second dead time consistent with manual data collection. Extinction coefficients were independently determined (Table 3) and fixed during fitting. Vertical scaling factors were used and fixed during fitting. Errors were calculated from 2D Fitspace at 0.83 Chi², with all scaling factors locked. Dopamine and 6-cyanodopamine were examined under oxygen-saturated (100%  $O_2$ ) and air-saturated (21%  $O_2$ ) conditions, while 6-bromodopamine and 6-carboxydopamine were evaluated under oxygen-saturated conditions only.